



HAWASSA UNIVERSITY

SCHOOL OF POSTGRAGUATE STUDIES

COLLEGE OF NATURAL AND COMPUTATIONAL SCIENCES

DEPARTMENT OF CHEMISTRY

**PHOTOCATALYTIC DEGRADATION OF CRYSTAL VIOLET
UNDER SOLAR IRRADIATION USING A BIOSYNTHEZIZED ZnO-
BASED POLYANILINE**

MSc THESIS

BY:

BELAYNESH SIRIYE TALILA

ADVISOR: ENDALE TSEGAYE (PhD)

MAY, 2024

HAWASSA, ETHIOPIA

**PHOTOCATALYTIC DEGRADATION OF CRYSTAL VIOLET
UNDER SOLAR IRRADIATION USING A BIOSYNTHEZIZED ZnO-
BASED POLYANILINE**

**A MASTER THESIS SUBMITTED TO THE SCHOOL OF
GRADUATE STUDIES OF HAWASSA UNIVERSITY, IN PARTIAL
FULFILLMENT OF THE REQUIREMENTS FOR THE DEGREE OF
MASTERS OF SCIENCE IN PHYSICAL CHEMISTRY**

BY

BELAYNESH SIRIYE

ID No; GPChmR/0004/15

ADVISOR: ENDALE TSEGAYE (PhD)

MAY 2024

HAWASSA, ETHIOPIA

HAWASSA UNIVERSITY
SCHOOL OF POSTGRAGUATE STUDIES
COLLEGE OF NATURAL AND COMPUTATIONAL SCIENCES
DEPARTMENT OF CHEMISTRY

DECLARATION

I declare that, this thesis “**Photocatalytic Degradation of Crystal Violet under Solar Irradiation Using a Biosynthesized ZnO-Based Polyaniline**” is my own work and I have duly acknowledged the sources of materials I have used.

Name: Belaynesh Siriye Signature: _____ Date: May, 2024

HAWASSA UNIVERSITY
SCHOOL OF POSTGRAGUATE STUDIES
COLLEGE OF NATURAL AND COMPUTATIONAL SCIENCES
DEPARTMENT OF CHEMISTRY

ADVISORS' APPROVAL SHEET

This is to certify that the thesis entitled '**Photocatalytic Degradation of Crystal Violet under Solar Irradiation Using a Biosynthesized ZnO-Based Polyaniline**' submitted to Department of Chemistry in partial fulfillment of the requirements for the **Master degree of sciences in Physical Chemistry** and has been carried out by **Belaynesh Siriye** under my supervision. Therefore, I recommended that the student has fulfilled the requirements and hence hereby can submit the thesis to the Department.

Advisor

Signature

Date

Endale Tsegaye (PhD)

HAWASSA UNIVERSITY

SCHOOL OF POSTGRAGUATE STUDIES

COLLEGE OF NATURAL AND COMPUTATIONAL SCIENCES

DEPARTMENT OF CHEMISTRY

EXAMINER'S APPROVAL SHEET

We the undersigned members of examiners of the final open defense by Belaynesh Siriye have read and evaluated his thesis entitled **Photocatalytic Degradation of Crystal Violet under Solar Irradiation Using a Biosynthesized ZnO-Based Polyaniline** and examined the candidate. This is, therefore to certify that the thesis has been accepted in partial fulfillment of the requirements for the master's degree.

Name of Major Advisor	Signature	Date
Name of Internal Examiner-I	Signature	Date
Name of Internal Examiner-II	Signature	Date
Name of External Examiner	Signature	Date
SGS Approval	Signature	Date

Final approval and acceptance of the thesis is contingent upon the submission of the final copy of the thesis to the school of graduate studies (SGS) through the department school committee (DGC/SGC) of the candidates department

Stamp of SGS	Stamp of Department	
Date	Date	

ACKNOWLEDGEMENTS

I sincerely thank my esteemed advisor, Endale Tsegaye (PhD), for his invaluable mentorship. His exceptional guidance, insights, and unwavering support have been instrumental in bringing this work to fruition. I am eternally grateful for his patience, encouragement, and belief in my abilities.

Special recognition goes to Prof. Sisay Tadesse (PhD) for his profound teachings and sharing of knowledge, which have profoundly shaped my intellectual journey. I am particularly indebted to Mr. Tilahun Tumiso, Mr. Yohannes Shuka, and Mr. Amanuel Abraham for their tireless contributions as laboratory specialists and research assistants. Their expertise and dedication ensured the smooth completion of the laboratory sessions and software analysis.

I extend my sincere appreciation to Mr. Wudineh Godero and my beloved family for their unwavering support and encouragement throughout my academic pursuit.

Finally, I express my gratitude to Wolaita Soddo University for the financial support that made this Master's degree in Physical Chemistry possible.

TABLE OF CONTENTS

DECLARATION	iii
ADVISORS' APPROVAL SHEET	iv
EXAMINER'S APPROVAL SHEET	v
ACKNOWLEDGEMENTS.....	vi
TABLE OF CONTENTS.....	vii
LIST OF TABLES	xi
LIST OF FIGURES	xii
LIST OF APPENDICES	xiii
ACRONYM AND ABBERVATIONS.....	xiv
ABSTRACT	xv
CHAPTER ONE	16
1. INTRODUCTION.....	16
1.1. Background of the Study	16
1.2. Statement of the Problem	18
1.3. Objectives	18
1.3.1. General Objective.....	18
1.3.2. Specific Objectives	18
1.4. Significance of the Study.....	19
1.5. Scope of the Study	19
CHAPTER TWO	20
2. LITERACTURE REVIEW.....	20
2.1. Environmental Pollutions and Toxicity of Dye	20
2.2. Nanoparticles.....	22

2.3. Types of Nanoparticles	23
2.3.1. Organic Nanoparticles.....	24
2.3.2. Inorganic Nanoparticles	24
2.3.3. Metal Nanoparticles	24
2.3.4. Metal Oxide Nanoparticles	24
2.3.5. Ceramic Nanoparticles	25
2.3.6. Biological Nanoparticles or Bio-nanoparticles	25
2.4. Zinc Oxide Nanoparticles	25
2.4.1. Modification of Zinc Oxide Nanoparticles	26
2.4.2. Conducting Polymer and Polyaniline (PANI)	27
2.4.3. Polyaniline Coupled ZnO NCs	28
2.5. Synthesis Methods of ZnO Nanoparticles	29
2.5.1. Physical Methods	29
2.5.2. Chemical Methods	30
2.5.3. Green Methods	30
2.6. <i>Solanecio gigas</i>	32
2.6.1. Descriptions of <i>Solanecio gigas</i>	32
2.6.2. Medicinal Values of <i>Solanecio gigas</i>	32
2.7. Photocatalytic Degradation	33
2.7.1. Photocatalysis	33
2.8. Experimental Parameters in Photocatalytic Degradation	35
2.8.1. Effect of Initial Concentration of Dye	35
2.8.2. Effect of pH.....	35
2.8.3. Effect of Photocatalyst Load.....	35
2.8.4. Effect of Temperature	36
2.8.5. Effect of Light Intensity and Wavelength.....	36

2.9. Kinetics of Photocatalytic Degradation.....	36
CHAPTER THREE	38
3. MATERIALS AND METHODS	38
3.1. Chemicals and Reagents	38
3.2. Apparatus, Equipments, and Instruments	38
3.3. Plant Material	38
3.4. Preparation of <i>Solanecio gigas</i> Extract	38
3.5. Green Synthesis of ZnO NPs.....	39
3.6. Chemical Synthesis of PANI and PANI/ZnO Composite.....	40
3.7. Characterization of ZnO NPs, PANI and PANI/ZnO NCs	40
3.8. Photocatalytic Degradation Study	40
3.9. Reusability Test.....	41
3.10. Kinetic Study for Photocatalytic Degradation	41
CHAPTER FOUR	42
4. RESULTS AND DISCUSSIONS	42
4.1. Green Synthesis of ZnO NPs	42
4.2. Characterization of Green Synthesized Nanoparticles	42
4.2.1. UV-Vis Analysis and Optical Study	42
4.2.2. FT-IR Analysis	46
4.2.3. SEM Analysis	48
4.2.4. XRD Analysis	50
4.3. Photocatalytic Activity Study	53
4.3.1. Effect of the Solution pH	53
4.3.2. Effect of Photocatalyst Dosage	54
4.3.3. Effect of Initial Concentration of CV.....	55
4.3.4. Effect of Reaction Time	57

4.4. Kinetic Study for Photocatalytic Degradation	58
4.4.1. Calibration Curve.....	58
4.4.2. Pseudo Zero, First, and Second-Order Kinetic Models	60
4.5. Mechanism of Photocatalytic Degradation	61
4.6. Nanocatalyst Reusability Test	63
CHAPTER FIVE	65
5. CONCLUSION AND RECOMMENDATION	65
5.1. Conclusion	65
REFERANCE	67
APPENDICES	75

LIST OF TABLES

Table 1: Optical band gap energy values of ZnO NPs, PANI powder and PANI/ZnO NCs	45
Table 2: XRD data used for calculation of crystalline size of Pure and PANI coupled ZnO NPs.....	52
Table 3: Rate constant (K) and correlation coefficient (R^2) calculated for the kinetic model	61

LIST OF FIGURES

Figure 1: Examples of chromophoric groups presents in organic dyes	21
Figure 2: Chemical structure of Crystal violet.....	22
Figure 3: Hexagonal-Wurzite structure of ZnO	26
Figure 4: Schematic diagrams extraction (Adopted [13]).....	31
Figure 5: <i>Solanecio gigas</i> Plant (Photo captured by Belayanesh S. on 10 Dec 2023).....	33
Figure 6: Photocatalytic degradation	34
Figure 7: Block diagram of <i>S.gigas</i> extract synthesis; sample collection (A), Washing (B), Drying (C), S.g powder (D), Heating (E), Filtration and Filtrate (F)	39
Figure 8: Color change.....	42
Figure 9: UV–Vis spectrum of pure ZnO NPs, PANI, and PANI/ZnO NCs.....	44
Figure 10: Tauc plot of pure ZnO NPs, PANI, & PANI/ZnO NCs	46
Figure 11: FTIR spectra S.g extract, Pure ZnO NPs, PANI, and PANI/ZnO NCs.....	48
Figure 12: SEM image of ZnO NPs (A), PANI (B) and PANI/ZnO NCs (C).....	49
Figure 13: XRD patterns of pure ZnO NPs, PANI, and PANI/ZnO NCs.....	51
Figure 14: Effect of pH of solution on photocatalytic degradation of CV	54
Figure 15: Effect nano photocatalyst dosage on photocatalytic degradation of CV.....	55
Figure 16: Effect of initial concentration of CV on photocatalytic degradation of CV.....	56
Figure 17: Effect of reaction time on the photocatalytic degradation of CV	58
Figure 18: Calibration curve of CV	59
Figure 19: Pseudo zero-order (a), pseudo-first-order (b) and pseudo-second-order kinetic models for the photocatalytic degradation of CV by ZnO NPs and PANI/ZnO NCs.....	61
Figure 20: Proposed mechanism for photocatalytic degradation.....	63
Figure 21: Reusability of pure ZnO NPs, & PANI/ZnO NCs nano catalysts for the degradation of CV	64

LIST OF APPENDICES

Appendix 1: Effect of pH.....	75
Appendix 2: Effect of photocatalytic dosage	78
Appendix 3: Effect of initial concentration of CV	79
Appendix 4: Effect of reaction time.....	80
Appendix 5: Calibration Curve data	82
Appendix 6: Kinetic data	83
Appendix 7: Nano-Catalyst Reusability.....	84

ACRONYM AND ABBERVATIONS

APS	Ammonium Peroxodisulfate
ASTM	American society for testing and materials
CV	Crystal Violet
EO	essential oil
FT-IR	Fourier-transform infrared
ICPS	intrinsic conducting polymers
JCPDS	joint committee on powder diffraction standards
MNPs	Metal nanoparticles
MONPs	Metal oxide nanoparticles
NCs	Nanocomposites
NPs	Nanoparticles
PANI	Polyaniline
SEM	scanning electron microscope
<i>S. gigas</i>	<i>Solanecio gigas</i>
UV-Vis	ultraviolet visible spectroscopy
XRD	X-ray-diffraction

ABSTRACT

A morphologically modified PANI/ZnO Nanocomposite was synthesized using leaf extract from Solanecio gigas (S. gigas) a reducing and capping agent for the photocatalytic degradation of Crystal Violet (CV) under natural sunlight irradiation. Additionally, PANI and pure ZnO NPs were synthesized via a green route, and the nanomaterials were characterized using spectroscopic techniques such as UV-Vis, FT-IR, SEM, and XRD. The blue-shift in the absorption peak of PANI/ZnO NCs suggests a change in electronic structure, potentially due to a type-II heterojunction between PANI and ZnO. FTIR analysis revealed red-shifted peaks, indicating hydrogen bonding between ZnO and PANI. Morphologically, the composite material combines the roughness of ZnO NPs with the smoothness of PANI. XRD patterns showed overlapping peaks from the composite with a crystalline size of 5.577 nm, which is smaller than the crystalline size of ZnO NPs (9.455 nm). This reduction in size is likely due to the formation of a polymer-Zn complex on the nanoparticle surface. The photocatalytic activity of the polyaniline/ZnO nanocomposite in degrading CV in aqueous solution under natural sunlight irradiation was evaluated and compared with that of ZnO nanoparticles. The effects of experimental conditions such as pH, photocatalyst dosage, and CV concentration were investigated with 91.20% and 99.06% at pH 11, 99.47% and 99.97% at 0.12 g, and 94.93% and 96.20% at 20 ppm for both ZnO NPs and PANI/ZnO NCs. The ZnO/polyaniline nanocomposite exhibited higher photocatalytic activity at 98.25% compared to ZnO nanoparticles at 92.76% under optimal conditions after 60 minutes of sunlight exposure. Kinetics studies indicated that the degradation rate fit well with the pseudo-first-order kinetics model, showing an R^2 value of 0.968 for PANI/ZnO NCs. The composite demonstrated good catalytic activity with four cycles of reusability time compared to non-coated ZnO NPs. These findings highlight the potential of S. gigas plant-assisted PANI/ZnO NCs as effective and sustainable nanocatalysts with promising applications in catalytic decomposition of organic contaminants for environmental remediation.

Keywords: *Crystal violet Dye degradation, Photocatalytic Activity, PANI/ZnO nanocomposite, S. gigas plant, Sunlight irradiation*

CHAPTER ONE

1. INTRODUCTION

1.1. Background of the Study

The increasing population has resulted in a significant rise in the contamination of surface and groundwater. One of the major sources of environmental pollution is organic dyes, which are commonly used in industries such as textiles and food. These dyes are non-biodegradable and highly toxic to aquatic organisms, as well as having carcinogenic effects on humans. Aromatic amines, such as crystal violet (CV), can easily enter the body through water or sweat absorption, making them particularly harmful to exposed areas like the skin and mouth. CV is widely used in industries such as textile and paper dyeing, as well as in printing inks and biological stains in veterinary and human medicine [1, 2].

Traditional methods like adsorption, flocculation, chemical oxidation, coagulation, ozonolysis, and ion exchange have been employed over the past few decades to treat polluted air and water systems. However, these methods have limitations in terms of sustainability and effectiveness [3]. In recent years, nanoscience and nanotechnology have played a crucial role in developing nanoparticles-based photocatalysts for degrading organic compounds in contaminated air and water. These photocatalysts aim to convert harmful organic dyes into harmless chemicals, thereby reducing the damage caused by dye pollution to the environment and human health [1].

Metal oxide nanoparticles, including ZnO [3, 4], TiO₂ [5], and CuO [6], have been extensively utilized in the photocatalytic degradation of non-biodegradable dyes. Researchers have focused on enhancing pollutant degradation rates by integrating inorganic materials with conductive polymers to leverage their synergistic and complementary properties [8]. Conductive polymers, known for their excellent hole-conducting abilities, serve as stabilizers or surface capping agents when combined with metal or semiconductor nanoparticles [9]. ZnO, a wide band gap semiconductor with a 3.37 eV band gap and a 60 meV exciton binding energy, exhibits potential for laser emission at room temperature due to its ability to capture high-energy photons, particularly UV light [2]. These properties make ZnO suitable for various optical and electronic applications, such as photovoltaic devices and solar cells. Polyaniline (PANI), a highly conductive polymer, is a promising material in polymer research due to its simple synthesis

process, high environmental stability, and diverse applications in electrochromic devices, light-emitting diodes, corrosion-resistant coatings, and electrostatic discharge protection[4], [10].

Numerous studies have focused on enhancing electron emission and photocatalytic activity of ZnO nanoparticles when combined with polyaniline conductive polymer through chemical and physical synthesis methods [11, 12]. However, these conventional approaches have limitations. To address this, the green synthesis of ZnO nanoparticles utilizing biological resources like plants, bacteria, algae, and fungi has garnered interest due to their abundant availability, cost-effectiveness, low toxicity, and ability to produce stable nanoparticles with precise sizes and shapes. Plant extracts serve naturally as reducing, stabilizing, and capping agents during the synthesis of nanoparticles [13].

The study aimed to investigate the comparative photocatalytic activity of pure ZnO nanoparticles and PANI/ZnO nanocomposites under natural sunlight irradiation for the degradation of Crystal Violet, utilizing a leaf extract of *Solanecio gigas* as a bioreducing and capping agent. *Solanecio gigas* belongs to the *Senecioneae* family of plants, which includes species including *Cacalia*, *Crassocephalum*, *Emilia*, and *Senecio*, all of which can biosynthesis hepatotoxic pyrrolizidine alkaloids. The plant's widespread use as natural medicine, as well as its taxonomic similarities to the well-studied *Senecio* species, sparked our interest in conducting scientific research on it [14]. The green synthesis of ZnO nanoparticles using biological resources like plants has gained attention for its ease of availability, low cost, low toxicity, and capacity for large-scale synthesis of stable nanoparticles with controlled size and shape. In this study, new *Solanecio gigas* extract-assisted ZnO nanoparticles, PANI, and PANI/ZnO nanocomposites were synthesized in an aqueous diethylene glycol solution via chemical oxidation of aniline for the first time. The surface structure and morphology of the synthesized materials were characterized using spectroscopic techniques. The photocatalytic activities of the green-synthesized ZnO nanoparticles and PANI/ZnO nanocomposites were evaluated by monitoring the degradation of CV dye under natural sunlight irradiation. The study also investigated the effects of organic dye type, irradiation time, photocatalyst amount, and the reusability of photocatalysts on the photocatalytic activity. This research demonstrates the potential for developing efficient and environmentally friendly photocatalysts for the removal of hazardous organic dyes from wastewater.

1.2. Statement of the Problem

Today, the environmental pollution jeopardizes the survival of life, driven by rapid urbanization and industrial growth. Its impact is strong on the developing countries like Ethiopia, due to low income and lack of wastewater management and treatment technologies. Industrial based pollutions stemming from various sources, including inorganic, organic, and organometallic compounds, poses a significant risk to ecosystems. Of particular concern are persistent organic pollutant dyes, known for their toxicity and harmful effects on the environment [1]. Over the last two decades, researchers have designed and applied various strategies to develop sustainable methods like green synthesis of ZnO nanoparticle for the photocatalytic degradation of toxic environmental pollutants over conventional methods [4]. However, these methods are challenged in photocatalytic efficiency due to their good absorption in the UV region of solar light, which constitutes small portion of the total radiation [2, 15]. Additionally, the synthesis of nanoparticles using physicochemical methods have been remain expensive, use of toxic, hazardous and non-ecofriendly chemicals, use of high pressure, temperature and energy, required complication operative conditions [16]. Therefore, this study aimed to develop a simple, cost-effective, eco-friendly, sustainable, and green method for environmental remediation and enhance the efficiency by using semiconductor surface structure modification with polyaniline. To the best of my knowledge, the green synthesis of ZnO NPs and PANI/ZnO NCs using the leaf extract of *S. gigas* by the simple green method had never been reported so far. To cover this gap and explore the role of *S. gigas* plant for environmental remediation in PANI/ZnO NCs matrix has a novelty, which was considered the best modification in both physiochemical property of ZnO semiconductor could be more suitable for solar light on a with efficient photocatalytic properties for sustainable degradation of toxic pollutant dyes.

1.3. Objectives

1.3.1. General Objective

The main objective of this study was to synthesize ZnO/PANI Nanocomposite using plant extract and evaluate the Photocatalytic degradation of crystal violet using the nanocomposites.

1.3.2. Specific Objectives

- ✚ To synthesize ZnO and ZnO/PANI nanomaterials using the leaf extract of *S. gigas*.

- ✚ To characterize the synthesized ZnO NPs, PANI, and ZnO/PANI using XRD, UV-Vis, SEM, and FT-IR techniques.
- ✚ To evaluate the photocatalytic activity of the synthesized pure ZnO and PANI/ZnO NCs against CV.

1.4. Significance of the Study

This study focused on the synthesis of PANI/ZnO nanocomposites to enhance photocatalytic efficiency in degrading the organic pollutant dye CV. Utilizing plant leaf extract from *S. gigas* as a reducing agent, the research aimed to modify the optical properties of ZnO through surface modification with polyaniline, facilitating sustainable and eco-friendly degradation of organic pollutants. Moreover, the findings of this research could be used for:

- ✚ Provided valuable insights into the impact of pollutants discharged from industries, particularly dyes, on ecosystems.
- ✚ Providing further awareness for researchers about the application of the green synthesized PANI/ZnO NCs and upgrading the knowledge about the PANI/ZnO NCs regarding its photocatalytic activity.
- ✚ It demonstrated simple, cost-effective, and eco-friendly methods for treating industrial effluents before their discharge into the ecosystem, promoting reuse.
- ✚ Served as baseline information for researchers, expanding their knowledge on modifying MONPs for enhanced photocatalytic activity, and highlighted the environmental application of *S. gigas*.

1.5. Scope of the Study

The scope of this study is to investigate the photocatalytic degradation of crystal violet under solar irradiation using a biosynthesized ZnO-based polyaniline and capping agent. The study aims to explore the potential of photocatalytic degradation of the organic pollutant dye (CV) under natural sunlight irradiation in order to contribute to the development of an efficient and sustainable photocatalyst for environmental remediation. Characterization of the synthesized ZnO nanoparticles, polyaniline (PANI), and ZnO/PANI composite was done using X-ray diffraction (XRD), UV-Vis spectroscopy, scanning electron microscopy (SEM), and Fourier-transform infrared spectroscopy (FT-IR) techniques.

CHAPTER TWO

2. LITERATURE REVIEW

2.1. Environmental Pollutions and Toxicity of Dye

We are in the era of urbanization and industrialization, which requires different domains of electronics, energy storage devices, ecological remediation, microbial inhibition, medical implants and optical appliances [17]. About 10,000 different commercial organic dyes and pigments exist and more than 7×10^5 tons are produced per year over the worldwide and have been used in many industries such as textiles, printing, leather, pulp, food and plastics, etc. Approximately, 10-15% of these dyes is released through effluents after dyeing processes and can cause the environmental pollution [18]. As these compounds are toxic and carcinogenic in nature, their impact on the environment and human health is a major concern. Furthermore, these dyes impart color to aqueous body by blocking the penetration of sunlight and dissolution of oxygen [19].

Generally, dyes are complex unsaturated aromatic compounds with accomplishing characteristics like color, intensity, solubility, fastness, and substantiveness. Dyes are substances that, when applied to a substrate provides color by a process that alters, at least temporarily, any crystal structure of the colored substances. Such substances with considerable coloring capacity are widely employed in the textile, pharmaceutical, food, cosmetics, plastics, photographic and paper industries. The dyes can adhere to compatible surfaces by solution, by forming covalent bond or complexes with salts or metals, by physical adsorption or by mechanical retention [20]. Unlike most organic compounds, dyes possess colour because they 1) absorb light in the visible spectrum (400–700nm), 2) have at least one chromophore (colour-bearing group), 3) have a conjugated system, i.e. a structure with alternating double and single bonds, and 4) exhibit resonance of electrons, which is a stabilizing force in organic compounds. When any one of these features is lacking from the molecular structure the colour is lost. In addition to chromophores, most dyes also contain groups known as auxochromes (colour helpers), examples of which are carboxylic acids, sulfonic acid, amino, and hydroxyl groups. While these are not responsible for colour, their presence can shift the colour of a colourant and they are most often

used to influence dye solubility [21]. Figure 1 shows examples of chromophoric group found in organic dyes.

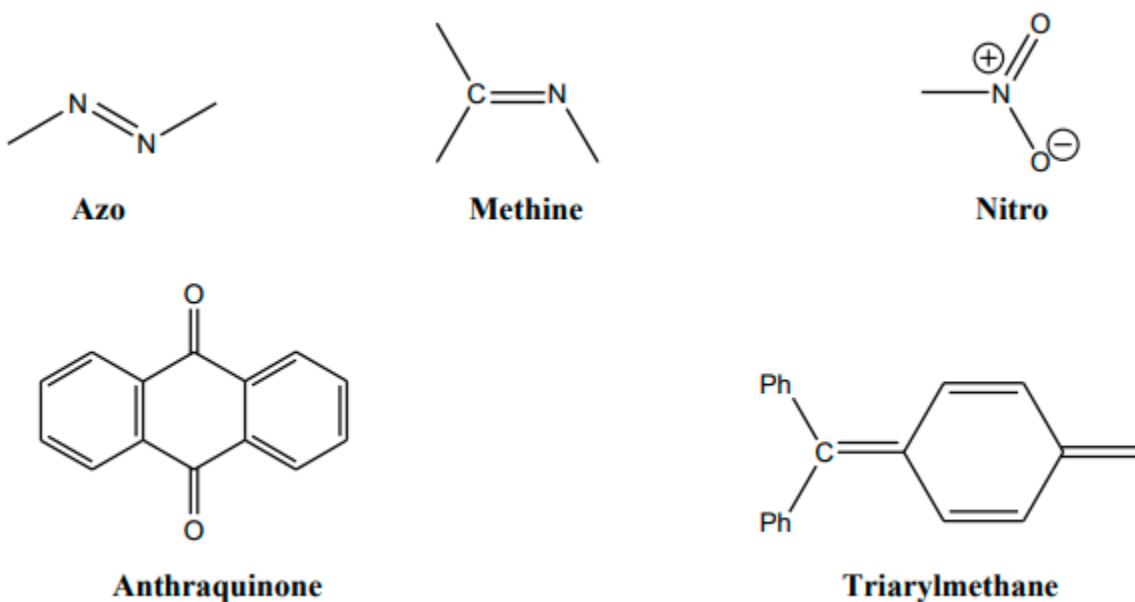


Figure 1: Examples of chromophoric groups presents in organic dyes

Crystal violet, chemically known as methyl violet 10B, is a synthetic dye with the formula $C_{25}H_{30}ClN_3$, characterized by its distinctive purple coloration (Figure 2). It is a member of the triphenylmethane family and has been extensively utilized in various applications due to its intense staining properties. In the field of microbiology, crystal violet plays a pivotal role in the Gram staining protocol, a fundamental technique for bacterial classification based on cell wall composition [22]. The dye's affinity for bacterial peptidoglycan allows for the differentiation between Gram-positive organisms, which retain the violet stain, and Gram-negative organisms, which do not. Beyond its diagnostic utility, crystal violet has also been employed in the textile industry as a fabric dye and in forensic science for fingerprint detection [23]

However, its widespread use has raised environmental concerns, particularly regarding water contamination. Studies have shown that crystal violet is recalcitrant to biodegradation, posing potential ecological and health risks [1]. Consequently, research efforts have been directed

towards developing sustainable methods for its remediation, such as adsorption techniques using low-cost and eco-friendly materials [23]. These studies not only aim to mitigate the environmental impact of crystal violet but also contribute to the advancement of green chemistry practices.

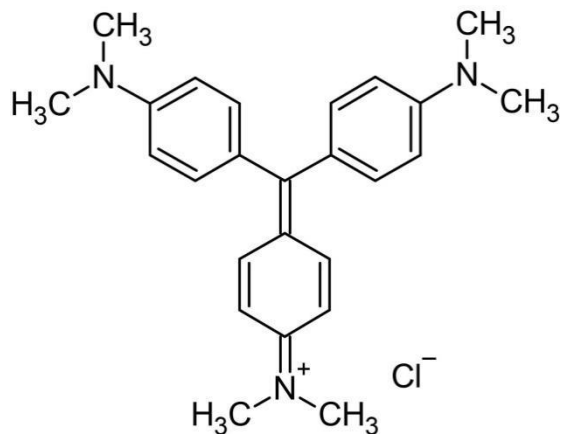


Figure 2: Chemical structure of Crystal violet

2.2. Nanoparticles

Nanotechnology is the technological innovations in the 21st century. Research and development in this field is growing rapidly throughout the world. A major contribution of this field is the development of new materials in the nanometer scale. Nanotechnology emerges from the physical, chemical, biological and engineering sciences where new techniques are being developed to probe and maneuver single atoms and molecules for multiple applications in different field of scientific world [24].

Nanoparticles are particles between 1 and 100 nanometers in size. In nanotechnology, a particle is defined as a small object that behaves as a whole unit with respect to its transport and properties. Particles are further classified according to diameter. Nanoparticle research is currently an area of intense scientific interest due to a wide variety of potential applications in biomedical, optical and electronic fields. The interesting and sometimes unexpected properties of nanoparticles are therefore largely due to the large surface area of the material, which dominates the contributions made by the small bulk of the material [25].

Nanoparticles, according to the ASTM standard definition, are particles with lengths that range from 1 to 100 nanometers in two or three dimensions [26]. A nanoparticle is defined as the smallest unit that can still behave as a whole entity in terms of properties and transport.

Nanoparticles are used in bio applications such as therapeutics, antimicrobial agents, drug delivery agents, biosensors, imaging contrast agents, transfection vectors, and fluorescent labels. Nanoparticles are of great scientific interest as they bridge the gap between bulk materials and atomic or molecular structures. A bulk material has constant physical properties regardless of its size, but at the nanoscale this is often not the case. Several well-characterized bulk materials have been found to possess most interesting properties when studied in the nanoscale.

Nanoparticles belong to the wider group of nanomaterials, where the prefix ‘nano’ refers to infinitesimal physical dimensions and where particles are defined as a “minute piece of matter with defined physical boundaries” where “physical boundary can also be described as an interface”. Many definitions have been proposed for nanoparticles and nanomaterials. Early definitions were based mainly on size, but with an increased understanding of the governing characteristics of nanomaterials, definitions have been refined. Definitions can be divided into two groups: regulatory and scientific. Regulatory definitions are often simplified to encompass the wide range of different nanomaterials in order to provide a common ground for discussion among regulators, industry and public. Some efforts are seen in the scientific literature to define nanoparticles based on their novel size-dependant properties. For example, it has been suggested that for inorganic nanoparticles, only particles of sizes below 30 nm exhibit properties that are different from the corresponding larger (bulk) particle of the same material.

A common definition of engineered nanoparticles, combining both size and property characteristics, is as particles with dimensions of about 1 to 100 nm, purposefully manufactured to have unique properties [27]. The chemical and physical properties of nanoparticles do not only depend on their size, but also on their composition which can be organic (polymers, lipids) as well as inorganic (metal, metal oxides, metalloid, metalloid oxides) or a mixture of both.

2.3. Types of Nanoparticles

The nanoparticles are classified into different types on the basis of morphology, size and shape. Some of the important classes of nanoparticles are mention in this review.

2.3.1. Organic Nanoparticles

The organic nanoparticles include ferritin, micelles, dendrimers and liposomes. The organic nanoparticles are not toxic, biodegradable and some organic nanoparticles have a hollow sphere i.e. micelles and Liposomes. It is also familiar with name of nanocapsules which are heat and light sensitive [28]. Organic nanoparticles are an ideal choice for drugs delivery due to these characteristics. Then nanoparticles are also widely used in target drug delivery. The organic nanoparticles are also known as polymeric nanoparticles. The most known shape of organic or polymeric nanoparticles is nanosphere or nanocapsule [29]. The matrix particles are former overall mass of which is solid and outer boundary of spherical surface adsorbs other molecules in the latter case, particles encapsulated the solid mass [30].

2.3.2. Inorganic Nanoparticles

Carbon is not present in inorganic nanoparticles. The inorganic nanoparticles are not toxic. The inorganic nanoparticles are biocompatible and hydrophilic. The inorganic nanoparticles are highly stable than organic. The inorganic nanoparticles are classified into metal and metal oxide nanoparticles [29].

2.3.3. Metal Nanoparticles

Metals are used to synthesize metallic nanoparticles by using destructive or constructive methods. The metal precursors are used to make the pure metal nanoparticles. The metal nanoparticles possess unique optoelectrical properties due to plasma resonance characteristics. The syntheses of metal nanoparticles are controlled by shape, facet and size [31]. The nanoparticles of all metals can be synthesized [32]. The nanoparticles of aluminum, gold, iron, lead, silver, cobalt, zinc, cadmium and copper are well-known metal nanoparticles. Nanoparticles exhibited distinctive properties due to the small size (10–100 nm), surface properties such as surface area to volume ratio, surface charge, pore size, surface charge density, structure (crystalline and amorphous), shapes (spherical, rod, hexagonal, tetragonal, cylindrical and irregular), color and environmental factor (sunlight, moisture, air and heat) [31].

2.3.4. Metal Oxide Nanoparticles

The purpose of the synthesis of metal oxide nanoparticles is to modify the property of their respective metals nanoparticles such as iron nanoparticles are oxidized to iron oxide

nanoparticles. The reactivity of iron oxides nanoparticles is increased as compared to the iron nanoparticles. Due to an increase in reactivity and efficiency of metal oxide, the nanoparticles of metal oxides are synthesized [33]. The example of metal oxide nanoparticles are zinc oxide, silicon dioxide, iron oxide, aluminum oxide, cerium oxide, titanium oxide and magnetite.

2.3.5. Ceramic Nanoparticles

Ceramic nanoparticles are also known as nonmetallic solid. The ceramics nanoparticles are synthesized via heating or successive cooling. The ceramic nanoparticles may polycrystalline, amorphous, porous, dense or hollow form [33]. The researchers focus on these nanoparticles due to their wide application such as photodegradation of dye, photocatalysis, catalysis and imaging applications [34].

2.3.6. Biological Nanoparticles or Bio-nanoparticles

Biological or Bio-nanoparticles is an assembly of atom or molecules which is prepared in the biological system having at least one dimension in the range of 1–100 nm. All bio nanoparticles are naturally occurring nanoparticles. These nanoparticles are dividing into two categories intracellular structure and extracellular structure. Magnetisms are an example of intracellular structure and lipoproteins and viruses are examples of extracellular structure. Magnetisms, exosomes, ferritin, lipoproteins and viruses are examples of bio nanoparticles [33].

2.4. Zinc Oxide Nanoparticles

ZnO is a wide band gap semiconductor material with a direct band gap of 3.37 eV and high binding exciton energy of 60 meV at room temperature. ZnO is an n-type semiconductor by nature due to the presence of intrinsic defects such as oxygen vacancies and Zn interstitials [35]. Zinc oxide nanoparticles (ZnO NPs) are one of the metal oxide nanoparticles which are nontoxic with refractive index of 2.0041. They are also hydrophobic inorganic compound existing in white powder form. The crystal structure of ZnO is in hexagonal-wurtzite as shown in Figure 3 where oxygen atoms (Purple spheres) are tetrahedral coordinated to Zn atom (Violet spheres).

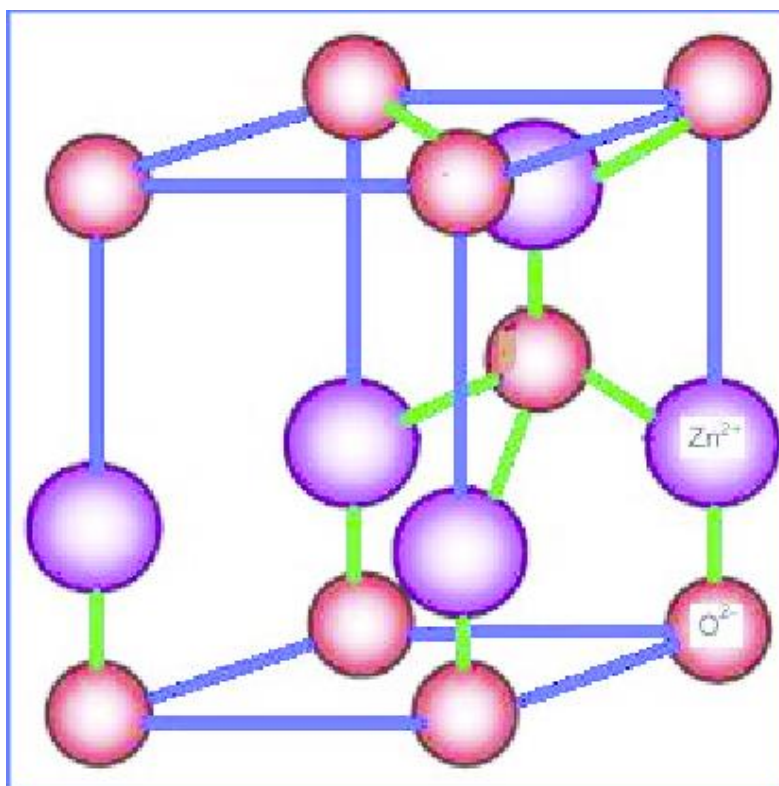


Figure 3: Hexagonal-Wurtzite structure of ZnO [36].

This structure contributes to the high piezoelectricity property. Piezoelectricity of ZnO arises from its crystal structure and makes it applicable for acoustic wave resonators and acoustic-optic modulators. Also, because of its Centro symmetric structure, it is the highest tensor among all semiconductors and gives large electromechanical coupling. ZnO nanoparticles are categorized as II-VI semiconductor as zinc and oxygen are from the 2nd and 6th group in periodic table, respectively. Thus, it can tolerate large electric fields, high temperature, and high power operations, high reflection rate, high photoelectric and non-linear optical coefficient [36].

2.4.1. Modification of Zinc Oxide Nanoparticles

Some modifications were implemented to enhance the applications of ZnO nanoparticles, for instance in hydrothermal method. This method involves the reaction of precursor chemicals in an aqueous solution under high pressure and temperature conditions, causing the precursor chemicals to react and form nanoparticles. Because of its low process temperature, eco-friendliness, low cost, scalability, use of basic equipment, and simplicity of handling, it is an

effective alternative synthetic technique that has attracted a lot of interest. When the temperature, duration, and precursor concentration of the hydrothermal process are altered, the shape and size of the particles can be adjusted. Controlling nanoparticle size, addition of surfactant, and doping with magnetic ions. Surfactant is a surface active agent who tends to reduce the surface tension of liquid and act as dispersant. Basically, it is an amphiphilic organic compound whereby it possesses both hydrophilic and hydrophobic characteristics. Indeed, it is proven that addition of surfactants is essential to prevent agglomeration. The presence of water molecules in ZnO nanoparticles leads to the formation of hard agglomerates. In order to setback this condition, surface modification with addition of surfactants were emphasized to increase their dispersibility [37].

Recent advancements in nanotechnology have led to significant interest in the modification of zinc oxide nanoparticles (ZnO NPs) due to their versatile applications in various fields, including medicine, electronics, and agriculture [38]. The modification of ZnO NPs often aims to enhance their functional properties, such as increasing their reactivity, stability, or compatibility with other materials. Techniques such as doping with other elements, surface functionalization, and composite formation have been explored to tailor the physicochemical characteristics of ZnO NPs for specific applications [39]. For instance, doping ZnO NPs with metals like silver or copper can impart antimicrobial properties, making them suitable for use in biomedical devices. Surface modification with organic molecules or polymers can improve the dispersibility of ZnO NPs in various solvents, which is crucial for their application in coatings or as additives in composite materials [38]. Furthermore, the incorporation of ZnO NPs into matrices like polymers or ceramics can result in composites with enhanced mechanical, thermal, or electrical properties [40]. These modifications not only expand the potential uses of ZnO NPs but also contribute to the development of more efficient and sustainable materials for future technological advancements.

2.4.2. Conducting Polymer and Polyaniline (PANI)

Conducting polymer composites are a suitable composition of a conducting polymer with one or more inorganic nanoparticles, so that their desirable properties are successfully combined successfully. Inorganic–organic composite materials are important due to their extraordinary properties, which arise from the synergism between the properties of the components. These

materials have gained much interest due to the remarkable change in properties such as mechanical, thermal, electrical, and magnetic compared to pure organic polymers [41]. Metal oxide-Polyaniline (PANI) nanocomposites have attracted significant attention due to their unique electrical, optical, and catalytic properties. These nanocomposites are promising materials for various applications such as sensors, energy storage devices, and environmental remediation.

In recent times, polyaniline (PANI) has gained significant attention as a conducting polymer due to its superior electrical and optical characteristics, enhanced air and water stability, and cost-effective synthesis process. These characteristics have led to the use of polyaniline in many different applications, including electrocatalysis, batteries, corrosion prevention, and separation membranes. Nevertheless, PANI's usefulness is restricted to acidic environments (pH less than 3), and the neutral polymer remains insoluble in standard solvents.

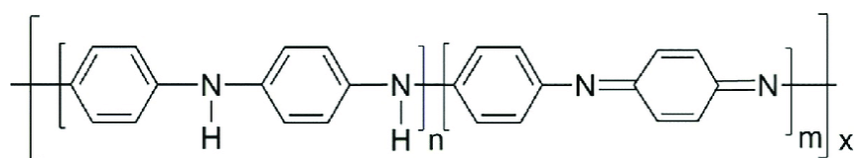


Figure 4: Polyaniline general formula

There are three distinct oxidation states for polyaniline. The oxidative polymerization of aniline in aqueous acids yields green protonated emeraldine, the most significant form of polyaniline. Because of the cation radicals in its structure, it has an electrical conductivity of $\sigma = 10^{-2}$ -100 S/cm [42]. Considerable thought has gone into creating processes for the synthesis of nanoparticles and nanocomposites of electroactive polymers with noble metals or metal oxides, based on the special benefits of nanosized materials. Based on this, metal nanoparticle–polyaniline composites, such as NiO/CuO/PANI graphene/PANI/polystyrene, were used to create electrochemical sensors [43].

2.4.3. Polyaniline Coupled ZnO NCs

The integration of polyaniline (PANI) with zinc oxide nanoparticles (ZnO NPs) has emerged as a promising approach in the field of material science, particularly for the development of advanced functional materials. The coupling of PANI, a conductive polymer, with ZnO NPs results in a

hybrid material that synergistically combines the unique properties of both constituents. The electrical conductivity of PANI, along with the semiconducting, photocatalytic, and antibacterial properties of ZnO NPs, makes this composite material highly suitable for applications in sensors, energy storage, and environmental remediation. The interaction between PANI and ZnO NPs can be tailored through various synthesis methods, such as in-situ polymerization or electrochemical deposition, which allows for the control of the composite's morphology and conductivity. Moreover, the PANI-coupled ZnO NPs have shown enhanced stability and selectivity, making them effective in detecting specific analytes in complex matrices. The ongoing research in this domain aims to optimize the synthesis process and to explore the full potential of PANI-coupled ZnO NPs in emerging technologies [44].

PANI/metal oxide nanoparticles composites can be exploited to store energy owing to the synergistic influence between PANI and metal oxides. P-Conjugated chain of ICPs, like PANI, is responsible for their pseudo capacitance and capacitance, which makes them outstanding electrode materials. On the other hand, the challenge of volumetric shrinkage and low conductance during the ejection of ions is overcome when the metal oxides are added. Surfactants have also been used as soft templates to achieve composite nanostructures [45].

2.5. Synthesis Methods of ZnO Nanoparticles

There are two approaches for synthesizing nanoparticles: "top-down" and "bottom up." The top-down approach the method involves breaking down large-scale bulk material into nanoscale particles, which can be achieved by several methods like as milling, attrition process, and electro explosion wire technique. Bottom-up approach Constructing a substance molecule by molecule, atom by atom, and cluster by cluster is known as the bottom method. Physical forces acting on the nanostructure employed to combine the particles into a bigger one during the assembly process [46]. Commonly, the synthesis methods are nanoparticles are classified in to three physical, chemical and biological.

2.5.1. Physical Methods

The physical methods for nanoparticle synthesis include thermolysis, physical vapor deposition (PVD), pulsed laser method, microwave-assisted synthesis, high energy ball milling, melt mixing, laser ablation, ion implantation, sputter deposition, electric arc deposition, etc. Each of

these methods changes one physical parameter; for instance, temperature is changed in thermolysis, pressure in ball milling, pH in ion implantation, laser ablation changes radiation, etc. The desired size and shape of the nanoparticles can be obtained by optimizing and maintaining the optimized parameters. However, primary disadvantages of physical methods include expensive equipment, time-consuming procedures, and higher parameters that are not favorable to the environment [46, 45].

2.5.2. Chemical Methods

Through chemical reaction processes, the chemical synthesis techniques used to produce metal oxide nanoparticles can be employed to produce more structured and complex nanomaterials. The reducing agent (chemicals) used in these methods are extremely reactive and poisonous substances such sodium borohydride and hydrazine hydrate, which can release hazardous byproducts that can negatively impact the environment, wildlife, and vegetation by releasing toxic by-products [47]. Chemical vapor deposition, sol gel, solvothermal process, polymerization, and another chemical precipitation techniques are examples of chemical methods for the synthesis of NPs. most of the chemical methods utilized to synthesize nanoparticles involve the use of hazardous and harmful chemicals, which can create biological risks, and sometimes these chemical processes are not favorable for the ecological environment.

2.5.3. Green Methods

Green chemistry is the design, development, and implementation of chemical products and processes that reduces or eliminates the use and manufacturing of substances that are harmful to the environment and human health. The green synthesis of MNPs and MONPs is one of the approaches that utilization biological systems and is based on green chemistry principle. Green synthesis of metallic nanoparticles has been adopted to accommodate various biological materials (e.g., bacteria, fungi, algae, and plant extracts). Using plant extracts is one of the greener ways to manufacture metal/metal oxide nanoparticles that is currently available. Compared to fungi and/or bacteria-mediated synthesis, this method is very easy and accessible to synthesis NPs at large scale. Green synthesis methodologies based on biological precursors depend on various reaction parameters such as solvent, temperature, pressure, and pH conditions (acidic, basic, or neutral). Green method is easy, economical, and environment friendly, and has gained a lot of importance in the recently. In green methods plant (Figure 4) material such as

fruits, leaves, flowers, roots, and seeds extract are used to synthesis metal oxide nanoparticle. For the synthesis of metal/metal oxide nanoparticles, plant biodiversity has been broadly considered due to the availability of effective phytochemicals in various plant extracts, especially in leaves such as ketones, aldehydes, flavones, amides, terpenoids, carboxylic acids, phenols, and ascorbic acids. These components are capable of reducing metal salts into metal nanoparticle [47, 48]. Successful green synthesis of ZnO NPs has been reported using a variety of plant components, including leaves, stems, roots, seeds, latex, fruits, interior plant parts, peels, and shells. Synthesized eco-friendly ZnO NPs using the aqueous extract of *Heliotropium indicum* aimed to evaluate the antimicrobial and photocatalytic activity [4].

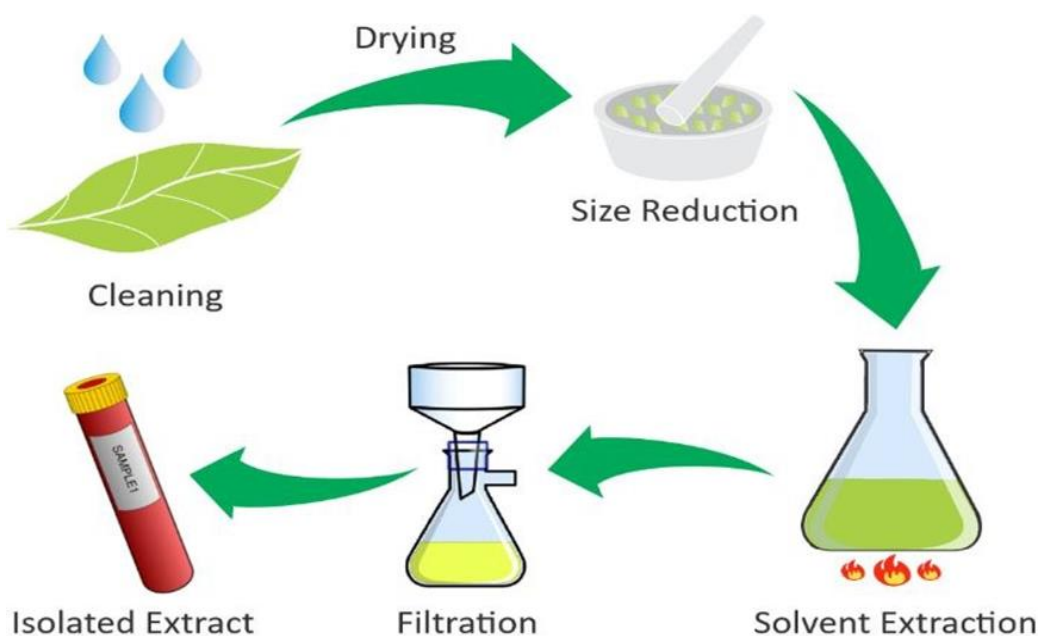


Figure 4: Schematic diagrams extraction (Adopted [13])

2.6. *Solanecio gigas*

2.6.1. Descriptions of *Solanecio gigas*

Within the sunflower family, the genus *Solanecio* comprises African plants belonging to the groundsel tribe [49]. The name "*Solanecio*" is a combination of the names "Solanum" and "Senecio," referring to the purported resemblance the species have to both of these established genera. Resemblance to *Solanum* is, of course, superficial [50]. *S. gigas* Plant shown in Figure 5 belongs to the *Senecioneae* family of plants, which includes species including *Cacalia*, *Crassocephalum*, *Emilia*, and *Senecio*, all of which can biosynthesis hepatotoxic pyrrolizidine alkaloids. The plant's widespread use as natural medicine, as well as its taxonomic similarities to the well-studied *Senecio* species, sparked our interest in conducting scientific research on it [51]. There were few scientific studies on this plant. Here, we report the composition and antibacterial and antioxidant activity of the essential oil (EO) and various extracts of *S. gigas* stem bark.

2.6.2. Medicinal Values of *Solanecio gigas*

One of Ethiopia's most important medicinal plants is *S. gigas* (Vatke) C. Jeffrey (*Asteraceae*) is a large rosette plant or shrub with soft woody stems that grows up to 4 meters tall. *S. gigas* is only found in Ethiopia, where it goes by the names "Yeshkoko-Gomen," "Abezenta," and "Nobe." It is also one of the most widely used plants in Ethiopian traditional medicine. The above ground whole plant is used to cure colic, diarrhea, gout, otitis media, typhus, wound dressing, anti-abortion, and mental faculty improvement (stems, leaves, and flowers). Extracts from the roots are also used to treat typhoid illnesses [14, 51].



Figure 5: *S. gigas* Plant (Photo captured by Belaynesh S. on 10 Dec 2023)

Active compounds found in plants have been shown to enhance the size, structure, and stability of synthesized nanoparticles. One such example is flavonoids, which are a class of polyphenolic chemicals that can effectively bind to metal ions and reduce them to nanoparticles [13].

2.7. Photocatalytic Degradation

2.7.1. Photocatalysis

Photocatalysis is defined as a photoinduced reaction which is accelerated by the presence of catalysts. These reactions activated by the absorption of a photon with the sufficient energy (equal or higher than the band-gap energy) of the catalysts [52]. The term photocatalyst is a combination of two words: photo related to photon and catalyst, which is a substance altering the reaction rate in its presence. Therefore, photocatalysts are materials that change the rate of a chemical reaction on exposure to light. This phenomenon is known as photocatalysis. Photocatalysis includes reactions that take place by utilizing light and a semiconductor. The substrate that absorbs light and acts as a catalyst for chemical reactions is known as a photocatalyst. All the photocatalysts are basically semiconductors.

Photocatalysis is a phenomenon, in which an electron-hole pair is generated on exposure of a semiconducting material to light. Absorption leads to a charge separation due to promotion of an electron from valence band of the semiconductor to the conduction band, thus generating a hole (h^+) in the valence band as shown in Figure 6. The recombination of the electron and the hole must be prevented as much as possible if a photocatalyzed reaction must be favored [53]. The ultimate goal of the process is to have a reaction between activated electrons with an oxidant to produce a reduced product, and also a reaction between the generated holes with a reductant to produce an oxidized product. The photo generated electrons could reduce the dye or react with electron accepters such as O_2 adsorbed on semiconductor surface or dissolved in water reducing it to superoxide radical an ion $O_2^{\cdot-}$. The photocatalytic reactions can be categorized into two types on the basis of appearance of the physical state of reactants. Homogeneous photocatalysis: When both the semiconductor and reactant are in the same phase, i.e. gas, solid, or liquid, such photocatalytic reactions are termed as homogeneous photocatalysis. Heterogeneous photocatalysis: When both the semiconductor and reactant are in different phases, such photocatalytic reactions are classified as heterogeneous photocatalysis [54].

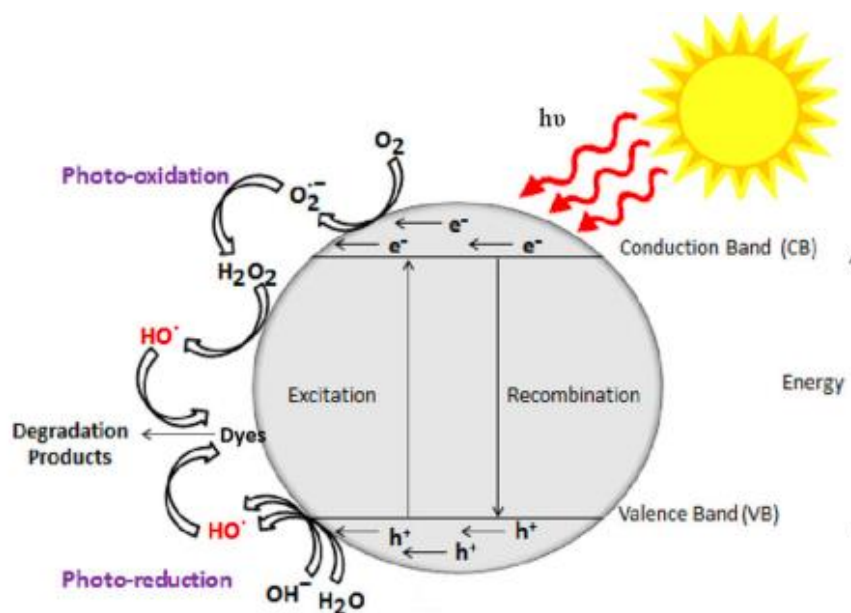


Figure 6: Photocatalytic degradation

2.8. Experimental Parameters in Photocatalytic Degradation

Several studies have been reported the significance of operational parameters. The photo degradation depends on the some basic parameters which are initial concentration of dyes, amount of photocatalyst, pH of the solution, temperature of reaction medium, the intensity of light, nature of the substrate, dopant. The oxidation rates and efficiency of the photocatalytic system are highly dependent on a number of operational parameters that govern the photo degradation of the organic molecule [55].

2.8.1. Effect of Initial Concentration of Dye

The photocatalysis is depends on the adsorption of dyes on the surface of photocatalyst. In the photocatalysis process, only the amount of dye adsorbed on the surface of photocatalyst contributes and not the one in the bulk of the solution. The adsorption of dye depends on the initial concentration of dye. The initial concentration of dye in a given photocatalytic reaction is an important factor which needs to be taken into account. Generally speaking the percentage degradation decreases with increasing amount of dye concentration, while keeping a fixed amount of catalyst [56].

2.8.2. Effect of pH

The Photo degradation of dyes is affected by the pH of the solution. The variation of solution pH changes the surface charge of semiconductor particles and shifts the potentials of catalytic reactions. As a result, the adsorption of dye on the surface is altered thereby causing a change in the reaction rate. The pH determines the surface charge of the photocatalyst. Adsorption of the dye is minimum when the pH of the solution is at the isoelectric point (point of zero charge). The surface of the photocatalyst is positively charged below isoelectric point and carries a negative charge above it [57].

2.8.3. Effect of Photocatalyst Load

Degradation of dye is affected by the amount of the photocatalyst. The photo degradation of dye increases with increasing catalyst amount, which is the feature of heterogeneous photocatalysis. The increase in catalyst amount actually increases the number of active sites on the photocatalyst surface thus causing an increase in the formation of number of \bullet OH radicals which can take part in actual discoloration of dye solution. Beyond a certain limit of catalyst amount, the solution

becomes turbid and thus blocks UV radiation for the reaction to proceed and therefore percentage degradation starts decreasing [1, 58].

2.8.4. Effect of Temperature

An increase in reaction temperature generally results in increased photocatalytic activity however reaction temperature $>80\text{ }^{\circ}\text{C}$ promotes the recombination of charge carriers and disfavours the adsorption of organic compounds on the semiconductor surface. Therefore temperature range between $20\text{-}80\text{ }^{\circ}\text{C}$ has been regarded as the desired temperature for effective photo mineralization of organic content [53].

2.8.5. Effect of Light Intensity and Wavelength

The intensity of light affects photodegradation and it determines the extent of light absorption by the semiconductor catalyst at a given wavelength. The degradation efficiency of dyes using a semiconductor photocatalyst depends on the intensity of light [59]. An increase in the intensity of light will result in increased photocatalytic reaction rates.

2.9. Kinetics of Photocatalytic Degradation

The kinetic study in photocatalytic degradation reaction involves the analysis of the rate of degradation of a target pollutant under optimum conditions. This includes the determination of the reaction rate constant, reaction order, and activation energy of the photocatalytic process. The study typically involves the use of a photocatalyst material, such as metal oxide, and a light source, such as UV light and visible to initiate the degradation reaction [6]. Based on the experimental data, mathematical models are developed to describe the degradation kinetics. These models often follow rate laws such as pseudo-zero order, pseudo-first order, and pseudo-second order, depending on the reaction mechanism.

A pseudo zero-order reaction thus is, observed for saturation coverage on the surface of the catalyst, since the catalytic degradation rate is independent of the change in the dye concentration, as shown in Equation (1);

$$[C]_0 - [C] = k_0 t \quad (1)$$

A plot of $[C]_0 - [C]$ vs reaction time gives a slope equal to the zero-order rate constant (k_0).

On the other hand, at low initial concentrations of dye molecules, i.e., $(K[C] + 1) = 1$, a pseudo first-order rate expression is obtained, as shown in Equation (2).

$$\ln \frac{[C]_0}{[C]_t} = k_1 t \quad (2)$$

The linear region can be obtained from the plot of $\ln([C]_0/[C]_t)$ versus reaction time, in which the slope gives the rate constant of degradation. A second-order reaction in which a single reactant is involved is characterized by the chemical reaction $(2[C] \rightarrow \text{products})$. Similarly, by integrating the equation under the two boundary conditions the second-order rate constant (k_2).

$$\frac{1}{[C]} - \frac{1}{[C]_0} = k_2 t \quad (3)$$

The Efficiency of **photo degradation** was calculated by using equation 4.

$$\text{Degradation Efficiency} = \frac{A_0 - A_t}{A_0} \times 100 \quad (4)$$

Where, A_0 is absorbance before degradation and A_t is absorbance of the dyes at a time t , on degradation.

CHAPTER THREE

3. MATERIALS AND METHODS

3.1. Chemicals and Reagents

In this study zinc nitrate hexahydrate [$\text{Zn}(\text{NO}_3)_2 \cdot 6\text{H}_2\text{O}$] (99.9%, CHD, India), were utilized as precursors. Sodium hydroxide, NaOH (99%, (GUJ), India) and hydrochloric acid, HCl (99%, Altiras, USA) were used for pH adjustment. Crystal violet (AR, Samir Tech-Chem, Ltd., India), a cationic dye, was chosen as the organic pollutant. Ethanol, CH_3OH was used for purification purpose. Aniline and Ammonium Peroxodisulfate (APS) from Merck Chemical Company, India were used for the polymerization. All chemicals and reagents used for the photocatalytic activity study were of analytical grade. Deionized water was employed to prepare all necessary solutions and for washing purposes throughout the experiment.

3.2. Apparatus, Equipments, and Instruments

A Muffle furnace (INSIF, India, Ho), an electric grinder, electronic balance, and common equipment such as a different types of flasks, plastic washing bottle, vial sample holder, beaker (SCHOTT DURAN, Germany), pH meter (CG 841, Germany), ceramic crucible, mortar and pestle, measuring cylinder (Superte, Borosilicate glass), Whatman no 1 filter paper (India), magnetic stirrer hot plate (INSIF, H-359), centrifuge (Labofuge 200, Germany), funnel, test tube (EIS, Pyrex glass), and metal stand setup were used for multipurpose tasks. The Ultraviolet-visible Spectrophotometer (SM-1600 spectrophotometer) was utilized for characterization and optimization.

3.3. Plant Material

The specimens of *Solanecio gigas* leaves were confirmed by Dr. Frew Mr. degafi and Mrs. abigiya a botanist in the Department of Biology at Hawassa University.

3.4. Preparation of *Solanecio gigas* Extract

A *Solanecio gigas* leaf was collected from Dobi Kebele in Gurage Zone, washed with distilled water, and dried at room temperature for 6 days (144 hours). Subsequently, the dried *S .gigas*

leaf was ground in an electric grinder to obtain a fine powder. Following this, 10 g of the powdered *S. gigas* was mixed with 100 ml of distilled water in an Erlenmeyer flask and heated at 80 °C while stirring using a magnetic stirrer for 30 minutes.

Finally, the heated *S. gigas* solution was allowed to cool for 20 minutes and filtered using whatman No. 1 filter paper to obtain a fine *S. gigas* extract solution, [60] in Hawwasa university instrumental laboratory as shown in Figure 7.



Figure 7: Block diagram of *S. gigas* extract synthesis ; sample collection (A), Washing (B), Drying (C), *S. gigas* powder (D), Heating (E), Filtration and Filtrate (F)

3.5. Green Synthesis of ZnO NPs

The experimental procedure reported by [59] was slightly modified to follow the green synthesis of zinc oxide nanoparticles. Briefly, 2.5 ml of *S. gigas* plant extract was added to 25 ml 0.5 M Zinc acetate dihydrate solution. The pH of the mixture was 6.13, 2 M NaOH was added drop wise to maintain pH at 8, then the mixture was then stirred and heated at 70 °C for 30 min for complete reduction and formation of a white precipitate. The aqueous extract of *Solanecio gigas* leaves, known to contain a variety of biomolecules [51], was utilized in this study. These phytochemicals possess diverse chemical and physical properties, such as antioxidant, lipid peroxidation, and metal ion reduction and stabilization capabilities. The *Solanecio gigas* aqueous leaf extract was employed to cap Zn^{2+} ions, leading to a noticeable color change The resulting

material was then collected via decantation, washed with distilled water to remove residuals and oven dried at 70 °C for overnight to yield powdered ZnO nanoparticles.

3.6. Chemical Synthesis of PANI and PANI/ZnO Composite

Binary PANI/ZnO nanocomposite preparation: 300 mL of hydrochloric acid (1 N) solution and 3 mL of aniline were combined, and the mixture was agitated for 35 minutes at room temperature. For the next ninety minutes, 0.6 g of ZnO nanoparticles were added and mixed once more. Subsequently, 6 g of APS was dissolved in 150 mL of 1 N HCl solution, creating a 150 mL APS solution, which was then combined drop-wise and agitated for the following 20 minutes. The mixture was then filtered, cleaned, and dried for five hours at 85 °C in an oven. For a comparative study, pure PANI was prepared by employing a similar process without mixing ZnO nanoparticles. [61].

3.7. Characterization of ZnO NPs, PANI and PANI/ZnO NCs

The formation of nanoparticles and nanocomposites was analyzed by UV-Vis Diffuse reflectance spectroscopy (JASCO V-670 UV – VIS) to elucidate and measure the optical properties in the range of 200–800 nm. The crystalline structure of green-synthesized ZnO NPs, PANI, and PANI/ZnO NCs was analyzed using an X-ray diffractometer (XRD- 7000, Shimadzu Corporation, Japan model) with a voltage of 40 kV and a current of 30 mA, using Cu K α = 1.5406 Å radiation as an X-ray source in the 2 θ range from 10° to 80°. The functional groups and metal-oxygen structure were analyzed by Fourier transform infrared (FT-IR) spectra of nanoparticles, which were recorded using a Perkin Elmer FT IR BX spectrophotometer in the range 4000–400 cm⁻¹ with samples prepared using KBr pellets. Scanning electron microscopy (SEM) was performed for morphological study using a JEOL - JSM-IT300L.

3.8. Photocatalytic Degradation Study

To investigate the photocatalytic degradation efficiency, 50 mL solution of 5 ppm CV dye in water was placed in 100 mL beakers, and 0.04 g of green synthesized ZnO nanoparticles was added as photocatalysts. The pH was then adjusted to 10, and the mixture was magnetically stirred in the dark for 30 minutes. After 30 minutes, the beaker containing the mixture was

exposed to direct sunlight irradiation with the highest light intensity selected from 11:30 a.m. to 3:00 p.m. for one hour. Following the photocatalysis reaction, the mixture was centrifuged to remove all nano-catalysts from the solution, and the absorbance of the CV solution before and after degradation was recorded at 590 nm using a UV–Vis spectrophotometer. The degradation efficiency of green synthesized ZnO nanoparticles was evaluated based on Equation 4. The same experimental procedure was repeated to optimize the photocatalytic activity parameters by varying different experimental parameters such as pH 2 – 14, the photocatalyst dosage (0.04, 0.08, 0.12, 0.16 and 0.20 mg), the initial concentration of CV dye (5, 10, 15, 20, and 25 ppm), and keeping all other parameters constant to investigate the optimum of one parameter by varying as stated. Effect of reaction time were investigated by withdrawing 5 mL aliquots of the mixture from the photocatalysis reaction every 10 minutes while the reaction occurred with all other photocatalytic parameters kept constant at the determined optimal point. Same procedure was repeated for evaluation of the photocatalytic performance PANI/ZnO NCs [4].

3.9. Reusability Test

The separation of the nanocatalyst from the photodegradation experiment was conducted through centrifugation, followed by washing with ethanol and deionized water. Subsequently, the nanocatalyst was dried at 80°C in an oven for two hours to ensure complete removal of residual moisture. The dried nanocatalyst was then subjected to reusability testing by undergoing four consecutive cycles under optimized experimental conditions of the photocatalytic degradation. After each cycle, the photocatalyst was reloaded with a consistent and concentration and amount of fresh CV dye to evaluate its stability and efficiency over four cycle uses. [62].

3.10. Kinetic Study for Photocatalytic Degradation

The photocatalytic degradation kinetics of CV dye on the surface of ZnO NPs and PANI/ZnO NCs were investigated using pseudo kinetics models such as pseudo-zero order, pseudo-first order, pseudo-second order, at various exposure times between 10 to 60 minutes. The experiments were conducted at optimized concentrations while keeping all other parameters constant. Linearized equations for pseudo zero-order, first-order, and second-order of kinetics, model (Eq. 1-3) respectively were employed in the analysis.

CHAPTER FOUR

4. RESULTS AND DISCUSSIONS

4.1. Green Synthesis of ZnO NPs

Alteration in color signifies the transformation of the reaction mixture into ZnO nanoparticles through nucleation, followed by the stabilization of the ZnO nanoparticles. Subsequent characterization of these nanoparticles using various techniques was conducted, and their potential photocatalytic activity was evaluated. A similar phenomenon was reported by Abomuti *et al.* [3], where color changes were observed due to the reduction of zinc salts by phytochemicals present in *Salvia officinalis* plant extracts, resulting in the formation of nanoparticles.



***S. gigas* Extract**

Zinc Nitrate Solution

Mixture

ZnO NPs

Figure 8: The color change of the solution mixture during synthesis of nanoparticles.

4.2. Characterization of Green Synthesized Nanoparticles

4.2.1. UV-Vis Analysis and Optical Study

The successful synthesis and optical properties of ZnO nanoparticles (NPs), polyaniline (PANI), and PANI/ZnO nanocomposites (NCs) were verified using UV-Vis spectroscopy, which enabled the assessment of their absorbance in the 200-800 nm wavelength range. The UV-Vis absorption

spectra presented in Figure 9 illustrate distinctive features for each material, allowing for an in-depth analysis of their electronic structure and photocatalytic potential.

ZnO NPs exhibit a prominent absorption peak in the UV region attributed to their wide band gap. The peak at approximately 305 nm corresponds to the band gap absorption of ZnO, signifying the transition of electrons from the valence band to the conduction band [63]. PANI typically displays an absorption peak in the UV region around 283 nm, associated with the π - π^* transition of its conjugated system [64]. In the case of the PANI/ZnO NCs, the presence of absorption peaks at 234, 283, and 340 nm indicates an interaction between PANI and ZnO NPs. This interaction suggests a modification in the electronic structure of ZnO, as evidenced by the shift in the absorption peak.

The observed blue-shift in the absorption peak towards lower wavelengths in the PANI/ZnO NCs signifies a change in the electronic structure, potentially arising from the formation of a type-II heterojunction between PANI and ZnO [65]. This heterojunction is anticipated to enhance charge separation and diminish the recombination rate of electron-hole pairs, thereby contributing to improved photocatalytic performance.

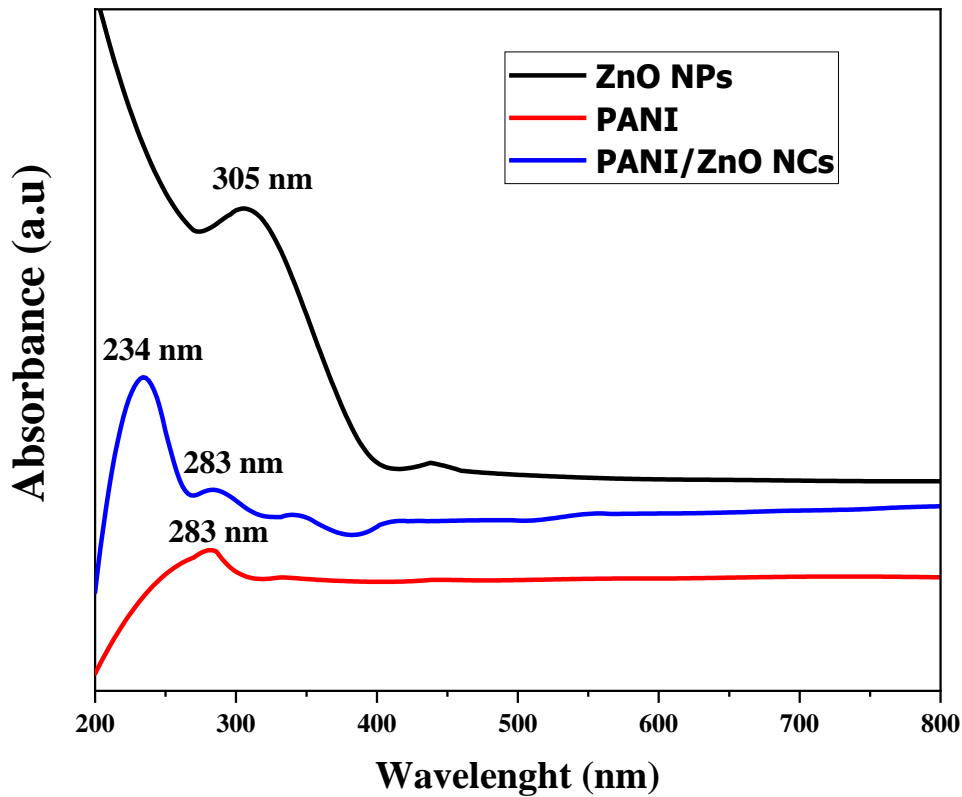


Figure 9: UV–Vis spectrum of ZnO NPs, PANI, and PANI/ZnO NCs

The band gap energy of green synthesized nanoparticles and nanocomposite was estimated through the application of the Tauc model. The optical band gap can be determined by using the well-known Tauc relation from equation (5)

$$(\alpha h\nu)^n = A(h\nu - E_g) \quad (5)$$

Where, A is a constant related to the material, α is the absorption coefficient in cm^{-1} , $h\nu$ is the photon energy in eV, E_g is the band gap energy in eV, and n is a constant that equals 2, 1/2, 2/3, and 1/3 for allowed direct, allowed indirect, forbidden direct, and forbidden indirect transitions, respectively. In this case, $n = 2$ is used for ZnO NPs and PANI, while $n=1/2$ for nanocomposite to determination of the optical band gap due to showing good linearity. The following formula [66] can be used to determine the material's band gap energy (E_g).

$$E_g (\text{eV}) = 1240/\lambda (\text{nm}) \quad (6)$$

Where, E_g is bang gap energy (eV), λ is wave length in (nm), corresponding to absorption edge.

As illustrated in Figure 10, the optical band gap (E_g) values were determined by extrapolating the linear portion of the plots of $(\alpha h\nu)^2$ vs. $h\nu$ are summarized in Table 1.

Table 1: Optical band gap energy values of ZnO NPs, PANI powder and PANI/ZnO NCs

Samples	E_{g1} (eV)	E_{g2} (eV)	E_{g3} (eV)
ZnO NPs	3.13	4.10	-
PANI	3.97	5.42	-
PANI/ZnO NCs	2.38	3.33	4.67

The UV-Vis absorption peak of zinc oxide nanoparticles (ZnO NPs) can shift when polyaniline (PANI) is coupled on their surface, indicating changes in the electronic structure and interactions between PANI and ZnO. This phenomenon, referred to as morphological modification, leads to a reduction in the bandgap from 3.13 to 2.38 eV and 4.10 to 3.33 eV. The coupling of PANI introduces new energy states within the bandgap of ZnO NPs, resulting in a narrowing of the bandgap. Consequently, the material can absorb light across a wider range of the visible spectrum, thereby enhancing its photocatalytic activity under visible light [67].

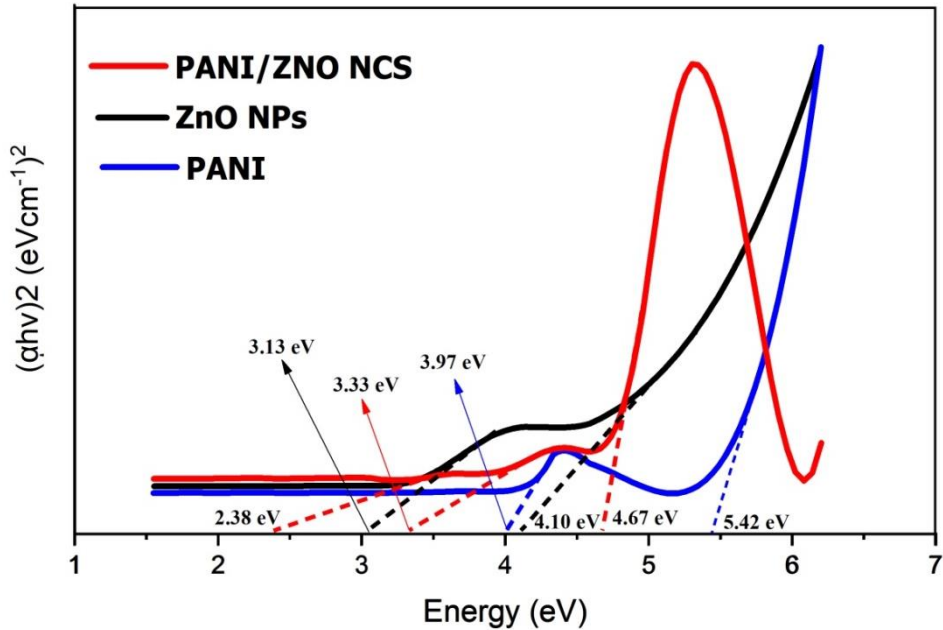


Figure 10: Tauc plot of ZnO NPs, PANI, & PANI/ZnO NCs

As depicted in Figure 10, PANI/ZnO nanocomposites have three band gaps due to the combination of two different materials with their own distinct band gaps. When these materials are combined at the nanoscale, their electronic properties can interact in such a way that the composite material exhibits multiple band gaps. Instead, it would exhibit a range of band gaps due to the combined electronic properties of PANI and ZnO. The specific band gap values, which are provided in a narrow range, are more likely to may represent the nanocomposites in the case of the targeted application, which is reducing the band gap to respond to photo detection.

4.2.2. FT-IR Analysis

The functional groups and Metal-Oxygen chemical bonds vibrational frequencies of *S. gigas* extract as well as green synthesized pure ZnO NPs, PANI, and PANI/ZnO NCs were identified through analysis of the FTIR spectra, as depicted in Figure 11. *S. gigas* Extract shows peaks at 3467, 2916, 2848, 1736, 1639, 1403, 1059, 676, and a small peak at 498 cm^{-1} could indicate the presence of various functional groups such as polyphenolic O-H, C-H stretching vibrations of methyl and methylene, primary N-H, carbonyl groups and C=C stretching vibrations in aromatic

rings respectively. This indicates the presence of biomolecules to capping during nanoparticle synthesis [13, 1, 4].

The FT-IR spectrum of ZnO NPs, exhibited characteristic peaks at 3467 and 2407 cm^{-1} could be attributed to the bending vibration of water molecules and air adsorbed on the ZnO surface, indicating hydroxyl groups and CO_2 , respectively. The peaks at 1629 and 1338 cm^{-1} may be represents the presence of primary C=C conjugation and C-O stretching where corresponding to the biomolecules from S.g extract during the biosynthesis, respectively. Interesting the peaks at 477 cm^{-1} for ZnO NPs corresponded to the characteristic stretching vibrations of the Zn-O bond [4, 63].

In the case PANI (Polyaniline), the major peaks are observed at 3469 corresponding to N-H stretching vibrations of secondary amine. The characteristic absorption bands of PANI are 505 cm^{-1} (C-N-C bonding mode of aromatic ring), 750 cm^{-1} (C-C, C-H bonding mode of aromatic ring), 810 cm^{-1} (C-H out of plane bonding in benzenoid ring), 1107 cm^{-1} (S=QO bonding for camphursulfonic acid), 1537 cm^{-1} (C-N stretching of benzenoid ring) and 1640 cm^{-1} (C=C stretching of quinoid ring (N=Q=N)) [68].

PANI/ZnO NCs exhibits major peaks at 3453, and 1522 cm^{-1} suggests broadening of hydrogen-bonded O-H stretching and C-O, indicating interactions between PANI and ZnO. Important peaks at 625 and 499 cm^{-1} revealed the formation of hydrogen bonding between ZnO and the -NH group of PANI [69, 70]. The infrared spectra of the PANI/ZnO NCs show minor band shifts towards the red side, but otherwise closely resembles that of the pure PANI. However, there is an evidence of peak displacement when ZnO nanorods are added to the PANI. These findings suggest that PANI and ZnO nanoparticles can interact in certain ways [71, 72].

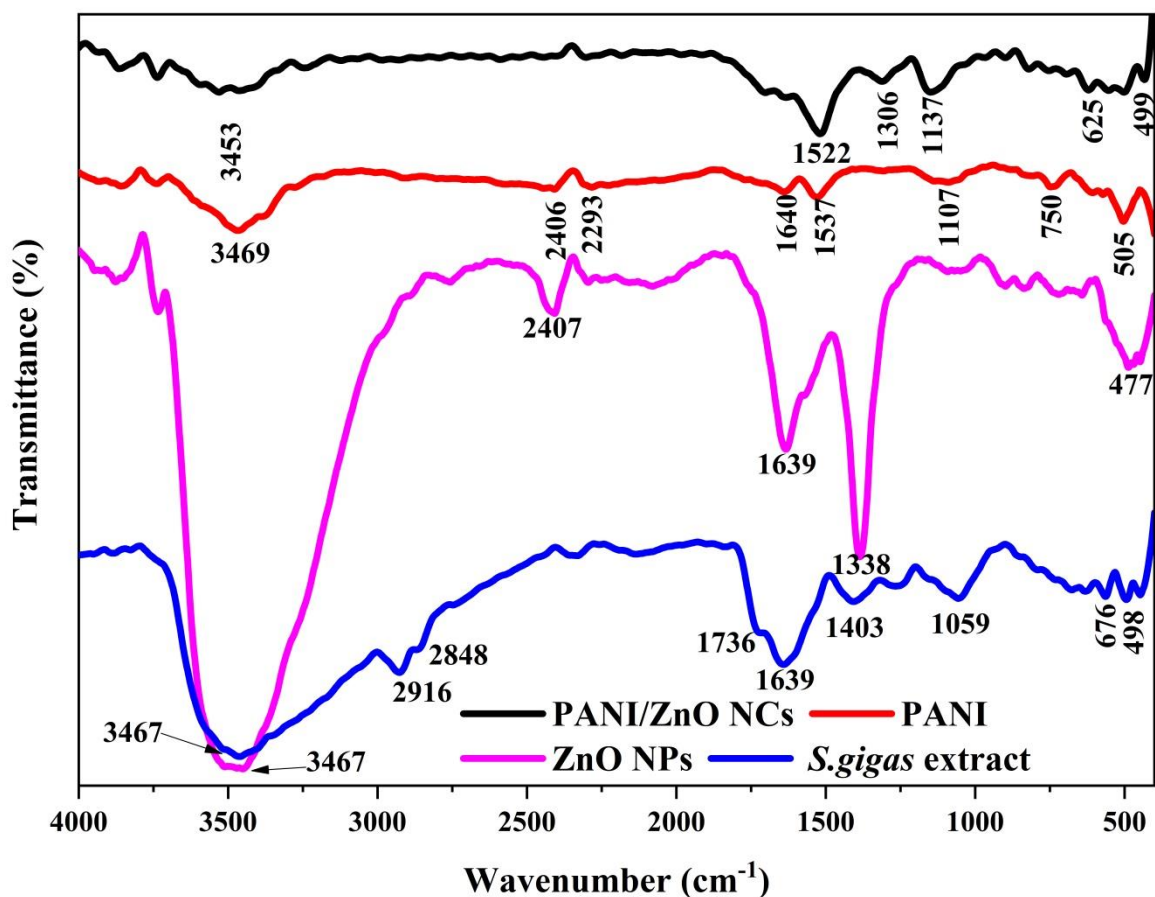


Figure 11: FT-IR spectra *S. gigas* extract, ZnO NPs, PANI, and PANI/ZnO NCs

4.2.3. SEM Analysis

The morphology and microstructure of green-synthesized pure ZnO nanoparticles (NPs), polyaniline (PANI), and PANI/ZnO nanocomposites (NCs) were examined using scanning electron microscopy (SEM) at a magnification scale of 10 μm , as illustrated in Figure 12. The SEM image (Figure 12A) of ZnO NPs reveals nanoflower and irregular shapes, consistent with previous findings reported by [8]. This morphology suggests a high surface area, which is advantageous for catalytic applications and reactivity enhancement. The rough and irregular features may indicate a synthesis method yielding particles with non-uniform shapes.

The morphology of pure PANI, depicted in Figure 12B, exhibits smoother surfaces, agglomerated, non-uniform, rough, and densely packed microstructures. The less defined

structures could be attributed to the use of strong oxidants and high aniline concentrations during the acidic PANI synthesis process, along with the inherent properties of polyaniline [71].

The intermediate texture observed between the roughness of ZnO NPs and the smoothness of PANI suggests a composite material (PANI/ZnO NCs). The morphology implies that PANI may be coating or interacting with ZnO nanoparticles, potentially influencing the material's electrical or optical properties as shown in Figure 12C. The intertwining of polyaniline on ZnO NPs significantly impacts the morphology of PANI/ZnO NCs and enhances the photocatalytic response [44].

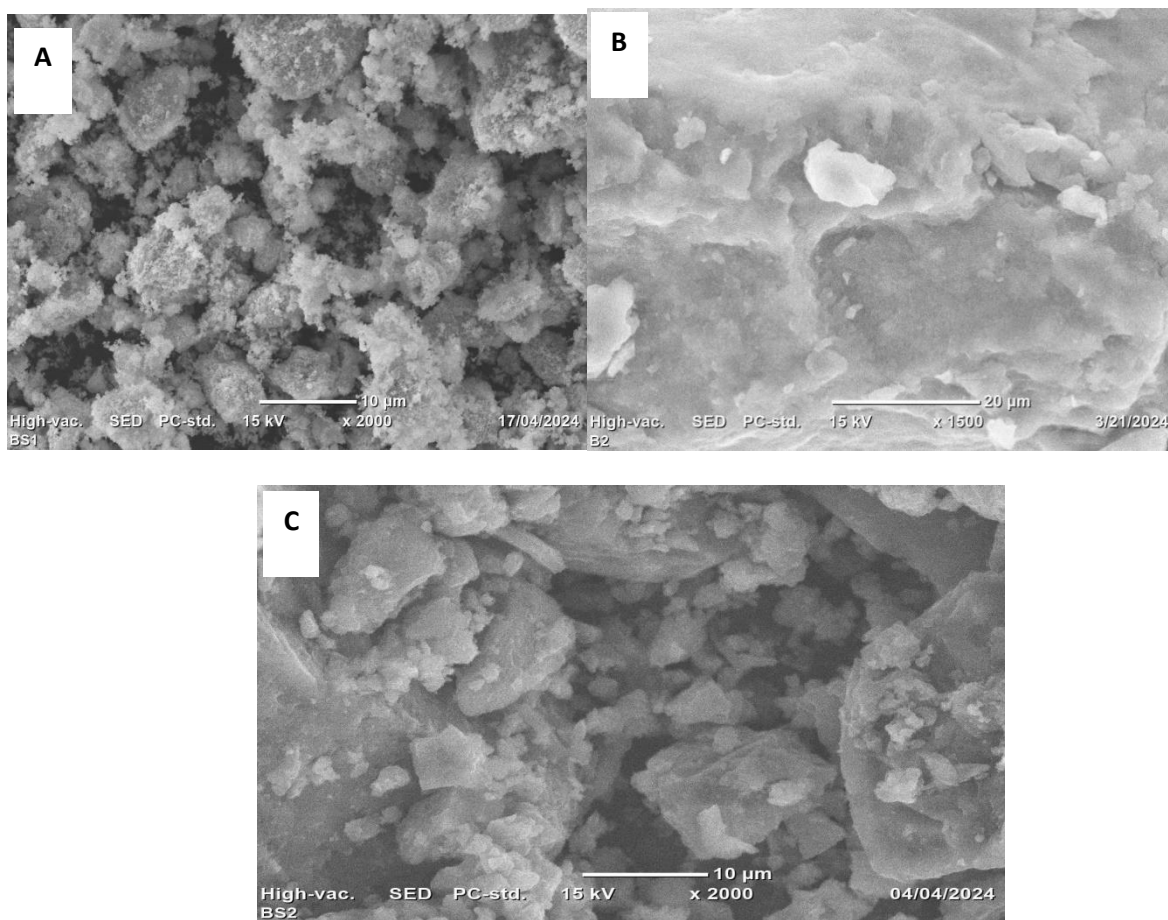


Figure 12: SEM image of ZnO NPs (A), PANI (B) and PANI/ZnO NCs (C)

4.2.4. XRD Analysis

X-ray diffraction (XRD) analysis was conducted to investigate the crystal structure and size of ZnO nanoparticles (NPs), polyaniline (PANI) powder, and PANI/ZnO nanocomposites. The XRD patterns for each nanomaterial are presented in Figure 13. The XRD pattern of ZnO reveals distinct peaks at 2θ values of 31.8° , 34.48° , 36.32° , 47.64° , 56.56° , 62.86° , 64.23° , 67.98° , 69.14° , and 75.32° corresponding to the (100), (002), (101), (102), (110), (103), (200), (112), (201), and (202) planes, respectively. These peaks align with the JCPDS reference number 01-079-2205, confirming the crystalline nature of ZnO NPs [4].

The XRD pattern of PANI displays broad peaks indicative of a semi-crystalline structure. Notably, peaks are observed at 20.48° and 25.38° corresponding to the (100) plane of quinoid units with π - π stacking-induced partial periodicity arrangement and the (110) plane of benzenoid units, consistent with literature reports on PANI [77]. The XRD pattern of the synthesized PANI/ZnO nanocomposites indicates a polycrystalline nature with a slight hint of amorphous characteristics. The XRD pattern shows overlapping peaks from both ZnO NPs and PANI, suggesting that the presence of polyaniline does not significantly alter the crystal structure of zinc oxide. However, the incorporation of PANI appears to reduce the size of ZnO nanoparticles, likely due to the formation of a polymer-Zn complex on the surface of the nanoparticles [75].

The XRD analysis reveals subtle shifts in the peak positions and intensities of ZnO NPs upon coupling with PANI, indicating changes in lattice parameters and potential interactions between PANI and the ZnO surface. The decrease in intensity of ZnO peaks suggests successful coupling with PANI, which may introduce some disorder at the nanoparticle surface [76]. These findings provide insights into the structural modifications induced by PANI coupling on ZnO NPs, offering valuable information for optimizing the properties of the composite for enhanced photocatalytic activity.

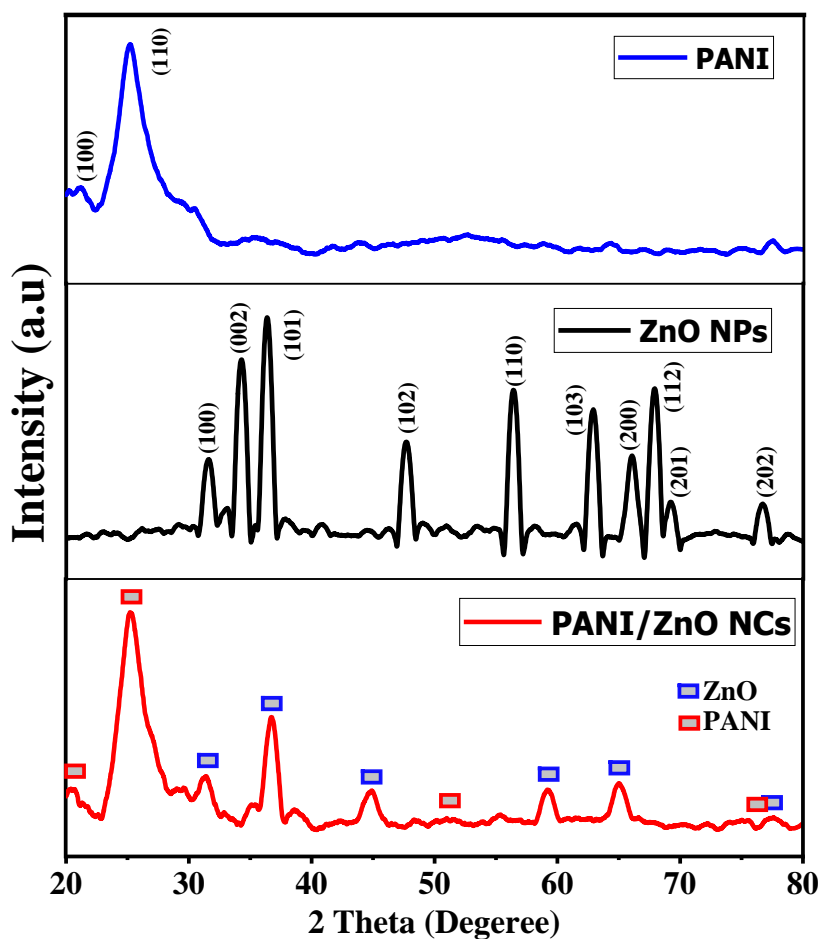


Figure 13: XRD patterns of ZnO NPs, PANI, and PANI/ZnO NCs

The broadening of the diffraction peaks observed during the coupling of PANI with ZnO NPs is attributed to the decreased crystallite size. To confirm this, the crystallite size of PANI, ZnO NPs, and PANI/ZnO NCs was calculated using the Debye–Scherrer Equation (7) as expressed by Patterson (1939). The full width at half maximum (FWHM) of the most intense diffraction peaks (002), (101), (102), (110), and (103) planes of ZnO NPs and (110) and (100) for PANI were measured and recorded in Table 2

$$D = \frac{K\lambda}{\beta \cos\theta} \quad (7)$$

Where, K is Scherrer constant (0.9), λ is wavelength of ZnO K α radiation (1.54056 nm), β is full width at half maxima (FWHM) of the diffraction peaks and 2θ is Bragg angle.

Notably, the average crystallite size of the ZnO NPs, PANI, and PANI/ZnO NCs was found to be 9.455, 2.200 and 5.577 nm, respectively. The decrease in crystallite size from pure to PANI-coupled ZnO is consistent with the data from UV-Vis, FT-IR, and SEM analyses previously discussed. The results indicated broadened diffraction peaks, suggesting that the lattice of the ZnO NPs is coated with PANI. This incorporation is anticipated to improve photocatalytic activity by modifying the surface structure of the host metal oxide. Similar findings reported by [75, 63] underscore the same findings for the PANI/ZnO matrix.

Table 2: XRD data used for calculation of crystalline size of Pure and PANI coupled ZnO NPs

Nano Catalysts	No	Miller indice s (<i>hkl</i>)	2θ (°)	FWHM (°)	Height of intensity (a.u)	Crystallite size (nm)	Average Crystallite size (nm)
ZnO NPs	1	002	34.26747	0.79657	495.88296	9.5305111	9.455
	2	101	36.36135	0.81428	607.74561	9.2691568	
	3	102	47.69888	0.74367	259.77689	9.7703753	
	4	110	56.41657	0.71373	415.20646	9.8087321	
	5	103	62.89825	0.71399	355.96578	9.492153	
	6	112	67.90104	0.74371	410.82006	8.8609108	
PANI	1	110	20.09984	3.28049	50.64016	2.384519	2.200
	2	002	25.49052	3.84233	152.93493	2.0166269	
PANI/ZnO NCs	1	002	19.11167	2.73878	25.11325	2.8604182	5.577
	2	101	25.44929	2.71546	101.85778	2.8537251	
	3	102	36.71147	1.04926	55.98701	7.1860933	
	4	110	44.79669	1.03746	15.38793	7.0797412	
	5	103	59.2327	0.93002	16.38535	7.4260757	

4.3. Photocatalytic Activity Study

4.3.1. Effect of the Solution pH

The impact of pH on the photocatalytic degradation of Crystal Violet (CV) using pure ZnO nanoparticles (NPs) and PANI/ZnO nanocomposites (NCs) was investigated across a pH range of 2–14, with consistent nano photocatalyst dosage, initial CV dye concentration, and irradiation duration. Optimal degradation efficiencies of 91.20% and 99.06% at pH 11 were observed for pure ZnO NPs and PANI/ZnO NCs, respectively, as detailed in Figure 14 and Appendix 1. The photocatalytic degradation efficiencies of CV by both nanocatalysts exhibited an increase up to the optimal pH of the solution, followed by a slight decrease, indicating the influence of the specific photocatalyst and pollutant utilized. This phenomenon arises from the surface charge of the nano photocatalysts, which are negatively charged in alkaline conditions (OH^-) and positively charged in acidic environments (H^+). Consequently, at lower pH levels in acidic media, protonation occurs on the nano catalyst surface, resulting in a positively charged CV dye, thereby enhancing the repulsive forces between the positively charged photocatalyst and the cationic dye, ultimately impacting the stability and activity of the nanocatalyst, leading to reduced efficiencies [4]. Conversely, efficiencies of CV were higher in alkaline media due to increased opposite-charge interactions between the solution and the nano photocatalyst surface caused by nano catalyst surface deportation [6]. Beyond the optimal pH, efficiencies decreased due to an excess availability of OH^- , leading to nanoparticle and nanocomposite destabilization. Consequently, pH 11 was identified as the optimized point for both nano photocatalysts for further experimental analysis.

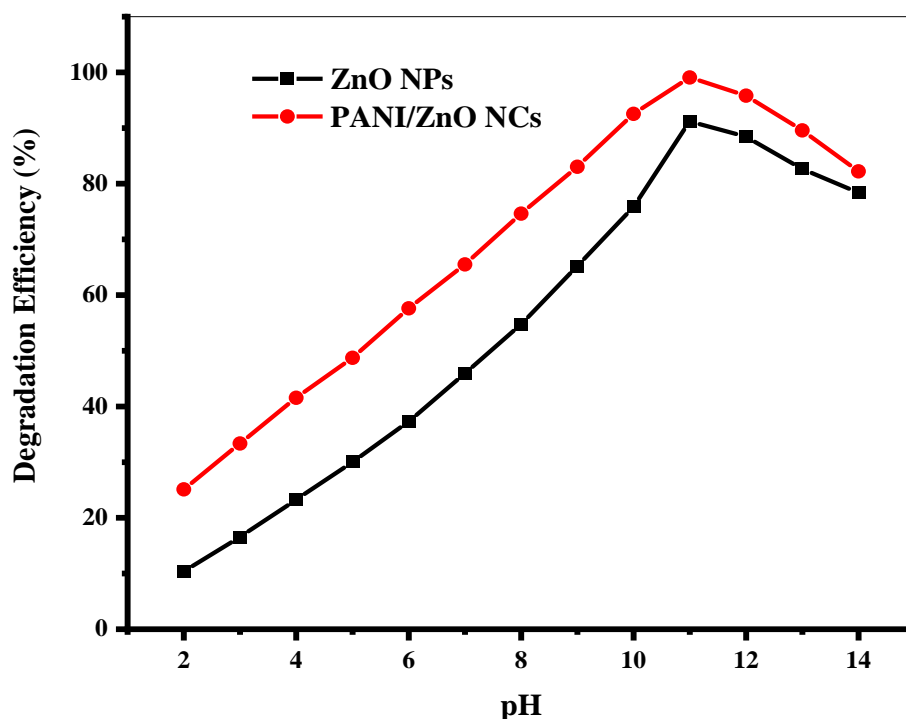


Figure 14: Effect of pH of solution on photocatalytic degradation of CV (5 ppm of initial conc. CV, 0.02 g of nano-photocatalyst dosage, $A_0 = 0.636$ and Exposure time = 60 min)

4.3.2. Effect of Photocatalyst Dosage

The impact of catalyst dosage on the photocatalytic degradation of Crystal Violet (CV) using pure ZnO nanoparticles (NPs) and PANI/ZnO nanocomposites (NCs) was investigated by varying the amount of photocatalyst load from 0.04 to 0.2 g with a 0.04 g interval, while keeping all other parameters constant. The results presented in Figure 15 and Appendix 2 indicate that an increase in the nano photocatalyst loading up to 0.12 g led to the maximum degradation efficiencies of 99.47% for pure ZnO NPs and 99.97% for PANI/ZnO NCs. This enhancement can be attributed to the greater accessibility of hydroxyl and superoxide radicals on the surface of active sites, resulting from the increased availability of electrons (e^-) and holes (h^+). However, a further increase in the photocatalyst dosage beyond the optimal point (0.12 g) for both pure ZnO NPs and PANI/ZnO NCs resulted in a decrease in the degradation rate. This decline may be attributed to factors such as nano photocatalyst aggregation, saturation of active sites, hindrance

and blocking of light penetration, and reduced availability of the degradable dye due to the excessive amount of photocatalyst dosage [1, 62]. Hence, a photocatalyst dosage of 0.12 g was selected as the optimal point for both nano photocatalysts for further investigation into the photocatalytic degradation of CV under sunlight

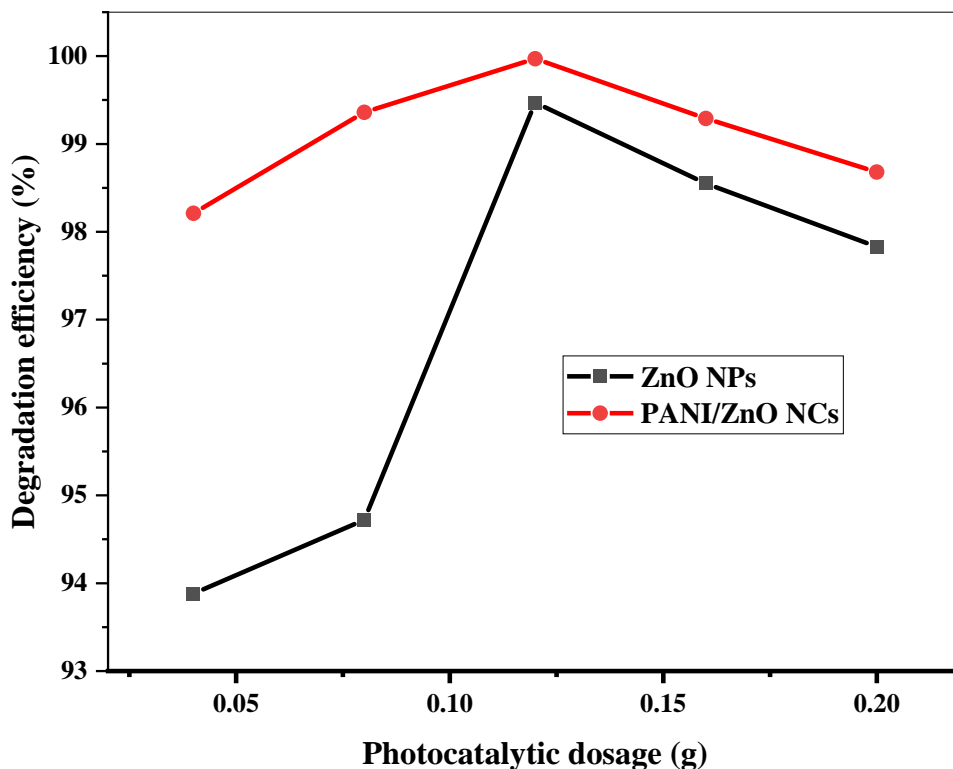


Figure 15: Effect nano photocatalyst dosage on photocatalytic degradation of CV (5 ppm of initial conc. CV, with optimized pH at 11 for ZnO NPs and 11 for PANI/ZnO NCs, respectively, $A_0 = 0.636$, and Exposure time = 1 hr.)

4.3.3. Effect of Initial Concentration of CV

The impact of the initial concentration of Crystal Violet (CV) in the solution on the photocatalytic degradation efficiency using pure ZnO nanoparticles (NPs) and PANI/ZnO nanocomposites (NCs) was investigated by examining five aqueous solutions with

concentrations ranging from 5 to 25 ppm at 5 ppm intervals, while maintaining all other parameters constant as optimized earlier. The results, as illustrated in Figure 16 and detailed in Appendix 3, indicated that the degradation efficiencies of pure ZnO NPs and PANI/ZnO NCs shows maximum degradation efficiencies 98.51 and 99.28% respectively, at initial concentration 5 ppm and decreased in minimal differences, as initial concentration of CV increased from 5 ppm to 20 ppm. This is because the nanoparticles have a large surface area available for adsorption and interaction with photons, resulting in more active sites. However, beyond 20 ppm the efficiency was exponential decrease. This decline can be attributed to the excessive amount of adsorbed CV, which could block active sites and reduce the interaction of light with these sites for hydroxyl radical generation. At higher dye concentrations, a significant portion of light may be absorbed by the dye molecules rather than by the photocatalysts, leading to a decrease in the formation of hydroxyl radicals and superoxide ions. Consequently, the degradation rate decreases with further increases in dye concentration [62, 77].

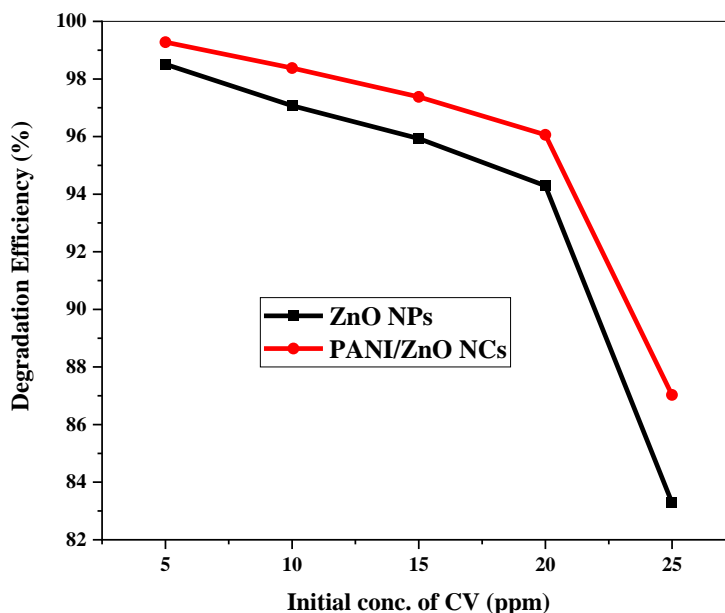


Figure 16: Effect of initial concentration of CV on photocatalytic degradation of CV (0.12 g for both ZnO NPs PANI/ZnO NCs and at with optimized pH at 11 for pure ZnO NPs and 11 for PANI/ZnO NCs, respectively and Exposure time = 1 hr.

4.3.4. Effect of Reaction Time

The impact of reaction time (irradiation) on the photocatalytic degradation of Crystal Violet (CV) by pure Zinc Oxide nanoparticles (ZnO NPs) and Polyaniline/Zinc Oxide nanocomposites (PANI/ZnO NCs) was investigated in this study. The degradation efficiencies were measured at 10-minute intervals of reaction times while maintaining all other parameters at their optimal points for each nanocatalyst, as previously discussed. The results, presented in Figure 17 and detailed in Appendix 4, revealed that the degradation efficiency of CV exhibited a sharp increase as the reaction time increased from the initial stage to the first 60 minutes of effective irradiation, reaching 92.76% and 98.25% for pure ZnO NPs and PANI/ZnO NCs, respectively. This enhancement can be attributed to the sufficient time required for maximum degradation, allowing the photocatalysts to effectively interact with the available CV and break it down through the proportional availability of active sites. However, beyond the 60-minute mark, further exposure to light did not result in any significant increase in degradation efficiency for all samples, indicating potential saturation or deactivation of active sites on the photocatalyst surface [6, 62].

Notably, the degradation efficiency of PANI/ZnO NCs (98.25%) surpassed that of pure ZnO NPs (92.76%). This increase in efficiency can be directly linked to the generation of electron-hole pairs, subsequently producing superoxide anions and hydroxyl radicals when light interacts with a semiconductor photocatalyst. These reactive oxygen species (ROS), resulting from bandgap reduction and an increased electron-hole transfer rate through surface modification with PANI, contribute to the degradation of dye molecules. The coupling of polyaniline (PANI) on the surface of zinc oxide nanoparticles (ZnO NPs) significantly enhances the photocatalytic degradation activity due to several factors: increased absorption extending to visible wavelengths, improved charge separation facilitating reduced recombination rates of electron-hole pairs, and a synergistic effect created by the combination of PANI and ZnO NPs, ultimately enhancing overall photocatalytic performance. [78-81].

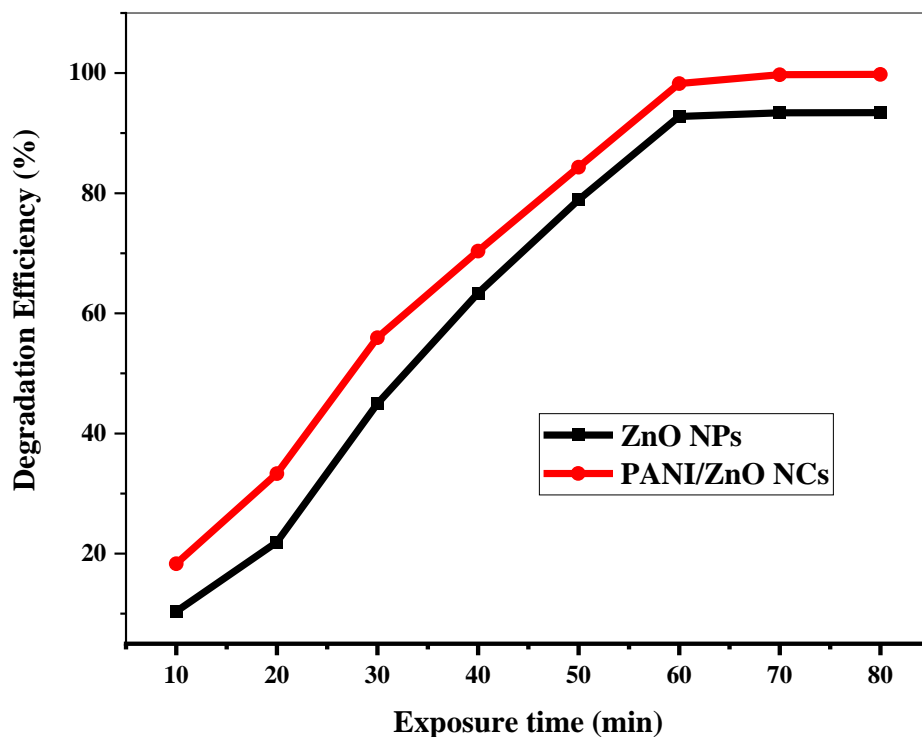


Figure 17: Effect of reaction time on the photocatalytic degradation CV (CV 20 ppm for both ZnO NPs PANI/ZnO NCs and at with optimized photocatalytic dosage 0.12 g, pH at 11 for pure ZnO NPs and 11 for PANI/ZnO NCs, respectively).

4.4. Kinetic Study for Photocatalytic Degradation

4.4.1. Calibration Curve

In this study, kinetic models were utilized to analyze the experimental data and elucidate the underlying degradation mechanism. Three kinetic models, namely pseudo-zero-order, pseudo-first-order, and pseudo-second-order, were employed to predict the degradation reaction data of dyes. The degradation kinetics experiments were conducted over varying reaction times ranging from 10 to 60 minutes under optimal experimental conditions, with all other parameters held constant.

To investigate the pseudo-kinetics, calibration curves were generated to calculate the dye concentrations after degradation at different time intervals based on Beer-Lambert's law. The calibration curves, depicted in Figure 18 (Appendix 5), facilitated the determination of dye concentrations at specific time points, allowing for the evaluation of the degradation rates and kinetics of the photocatalytic process. By fitting the experimental data to these kinetic models, insights into the degradation mechanism and reaction kinetics of the dyes could be obtained, providing valuable information on the efficiency and performance of the photocatalysts in degrading the target pollutants.

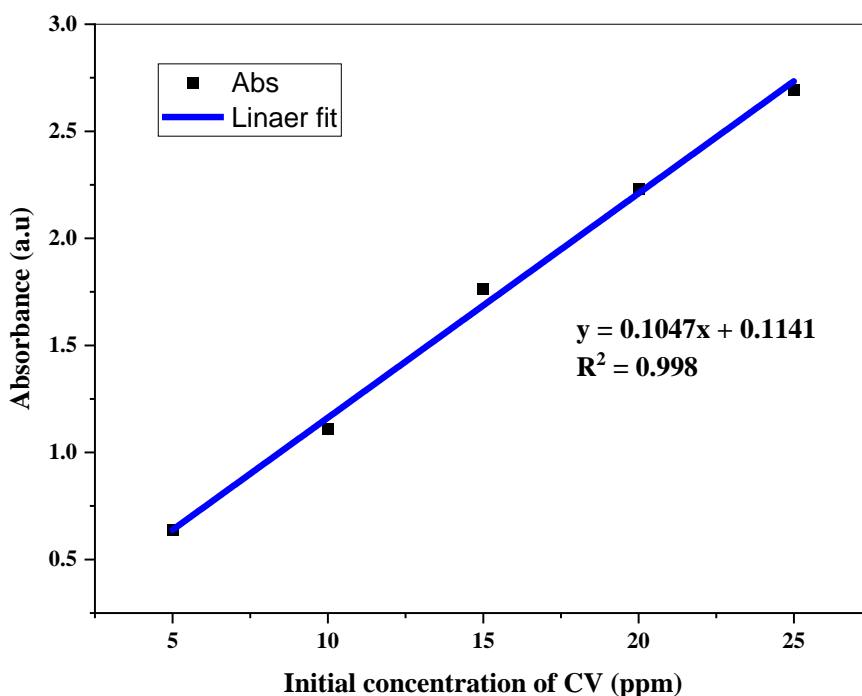


Figure 18: Calibration curve of CV

The pseudo kinetics experiments were conducted, the data used for calculating the residual concentration of the dyes and the final concentration of both dyes were calculated using their respective calibration curves, and other quantities used for investigating the pseudo kinetics were calculated and are shown in Appendix 6.

4.4.2. Pseudo Zero, First, and Second-Order Kinetic Models

To investigate the degradation kinetics of CV dyes facilitated by ZnO NPs, and PANI/ZnO NCs, linearized Equations (1), (2), and (3) were used. The plots were constructed as follows: plot of $C_0 - C_t$ against time (t), plot of $\ln [C_0/C_t]$ against time, and plot of $1/C_0 - 1/C_t$ versus time (t) and were utilized to analyse the pseudo-zero-order, pseudo-first-order, and pseudo-second-order kinetics models, respectively and are illustrated graphically in Figure 19 (a, b, and c). The correlation coefficients and rate constant for each kinetics model were determined and stated in Table 3.

The analysis of the data presented in Table 3 reveals that a high correlation coefficient close to unity ($R^2 = 0.957$) was achieved for Pure ZnO NPs when employing the pseudo zero-order kinetics model, while PANI/ZnO NCs exhibited an R^2 value of 0.968 with the pseudo-first-order kinetics model for the degradation of CV under natural sunlight. These results indicate that the photocatalytic degradation process of CV on the surfaces of Pure ZnO NPs and PANI/ZnO NCs align well with the pseudo zero-order and pseudo-first-order kinetics models, respectively. In contrast, the correlation coefficients for the other pseudo kinetics models were lower for both the nanoparticle and nanocomposite, as outlined in Table 3, suggesting a lack of conformity between these models and the actual degradation mechanisms of the dyes. These observations emphasize the robustness and reliability of the pseudo zero-order and pseudo-first-order kinetics models in elucidating the degradation pathways of various dyes when combined with specific nanocomposites. Ultimately, the results indicate that the pseudo-first-order kinetic model is most suitable for describing the degradation kinetics of CV by PANI/ZnO NCs. This conclusion is significant as it underscores the potential of ZnONPs as effective catalysts for dye degradation in applications related to wastewater treatment.

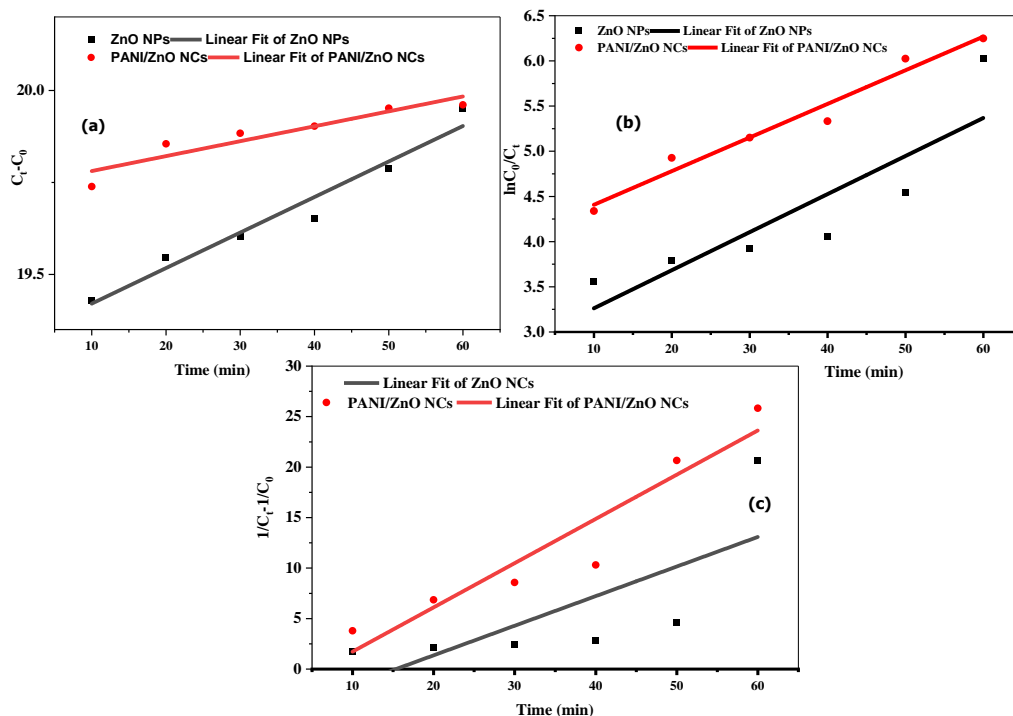


Figure 19: Pseudo zero-order (a), pseudo-first-order (b) and pseudo-second-order kinetic models for the photocatalytic degradation of CV by ZnO NPs and PANI/ZnO NCs

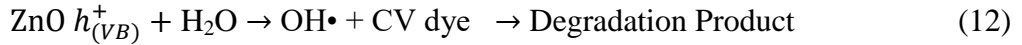
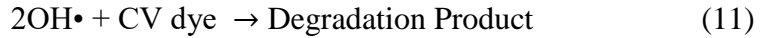
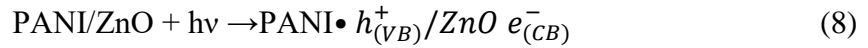
Table 3: Rate constant (K) and correlation coefficient (R^2) calculated for the kinetic model

Nano photocatalysts	Types of kinetics model					
	Pseudo zero order		Pseudo first order		Pseudo second order	
	K	R^2	K	R^2	K	R^2
ZnO NPs	0.009	0.957	0.042	0.766	0.293	0.553
PANI/ZnO NCs	0.004	0.879	0.037	0.968	0.438	0.903

4.5. Mechanism of Photocatalytic Degradation

Based on the experimental findings in this investigation, the potential mechanism underlying the photocatalytic reactions of ZnO and PANI/ZnO nanocomposite during the photocatalytic activity of PANI/ZnO under visible light irradiation can be anticipated as depicted in Figure 20. In the

presence of visible light irradiation, ZnO alone does not exhibit significant photocatalytic activity due to its high band gap leading to electron recombination. However, visible light absorption and photocatalytic behavior were observed upon modification of the ZnO nanoparticle surface with a PANI photosensitizer [80]. Upon exposure to visible light, the PANI molecules are excited, transferring electrons to the conduction band of ZnO nanoparticles (Eq. 8). The electrons in the conduction band of ZnO can catalyze the reduction of molecular oxygen, generating the superoxide anion radical (Eq. 9). This radical may further react to form hydrogen peroxide or organic peroxides in the presence of oxygen and organic molecules (Eqs. 10). An alternate pathway involves the generation of hydrogen peroxide, which can subsequently produce hydroxyl radicals, potent oxidizing agents (Eqs. 10 and 11). The resulting radicals have the capability to attack organic pollutants, forming intermediates that interact with hydroxyl radicals to yield the photocatalytic products [80], as described in equations (8-12) below;



The photocatalytic activity of ZnO nanoparticles under UV irradiation is enhanced by the presence of PANI, leading to a synergistic effect on the degradation of dye molecules. PANI facilitates the transfer of photogenerated holes from ZnO to the dye molecules, while the electrons in the conduction band of ZnO react with oxygen to produce superoxide anion radicals, contributing to dye degradation. The combination of PANI and ZnO extends the excitation wavelength towards the visible light region and delays electron-hole recombination, thereby increasing the overall efficiency of photocatalytic activity. These findings shed light on the complex mechanisms driving the degradation processes in PANI/ZnO nanocomposites under visible light irradiation, underscoring their potential for applications in environmental remediation [35, 78].

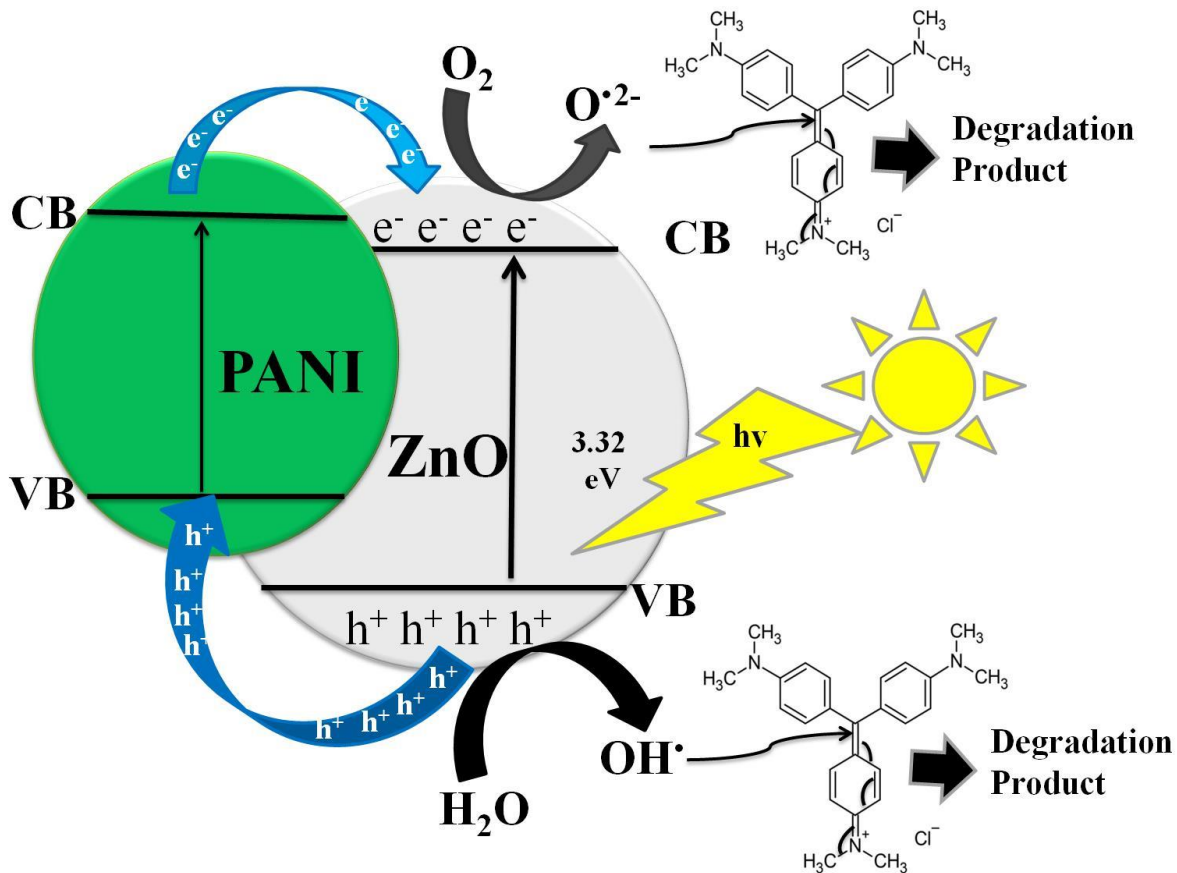


Figure 19: Proposed mechanism for photocatalytic degradation of CV by PANI/ZnO NCs

4.6. Nanocatalyst Reusability Test

Figure 21 and Appendix 7 depict the cyclic utilization of ZnO nanoparticles (NPs) and polyaniline/ZnO nanocomposites (PANI/ZnO NCs) for the degradation of crystal violet (CV) dye solution under UV light exposure. The results confirm that the PANI/ZnO nanocomposite maintains robust photocatalytic activity even after four cycles, highlighting its sustained efficiency. In comparison to the reusability of ZnO NPs, the efficiency of PANI-modified ZnO nanocomposites exhibits a slight decline with increasing cycle numbers (First cycle: 99.75%, Second cycle: 98%, Third cycle: 97.36%, Fourth cycle: 95.82%). These results suggest that the surface modification of ZnO NPs with PANI not only enhances photocatalytic activity but also improves catalytic stability. These findings underscore the potential of *S. gigas* plant-assisted

PANI/ZnO NCs as effective and sustainable nanocatalysts with promising applications in the catalytic decomposition of organic contaminants for environmental remediation."

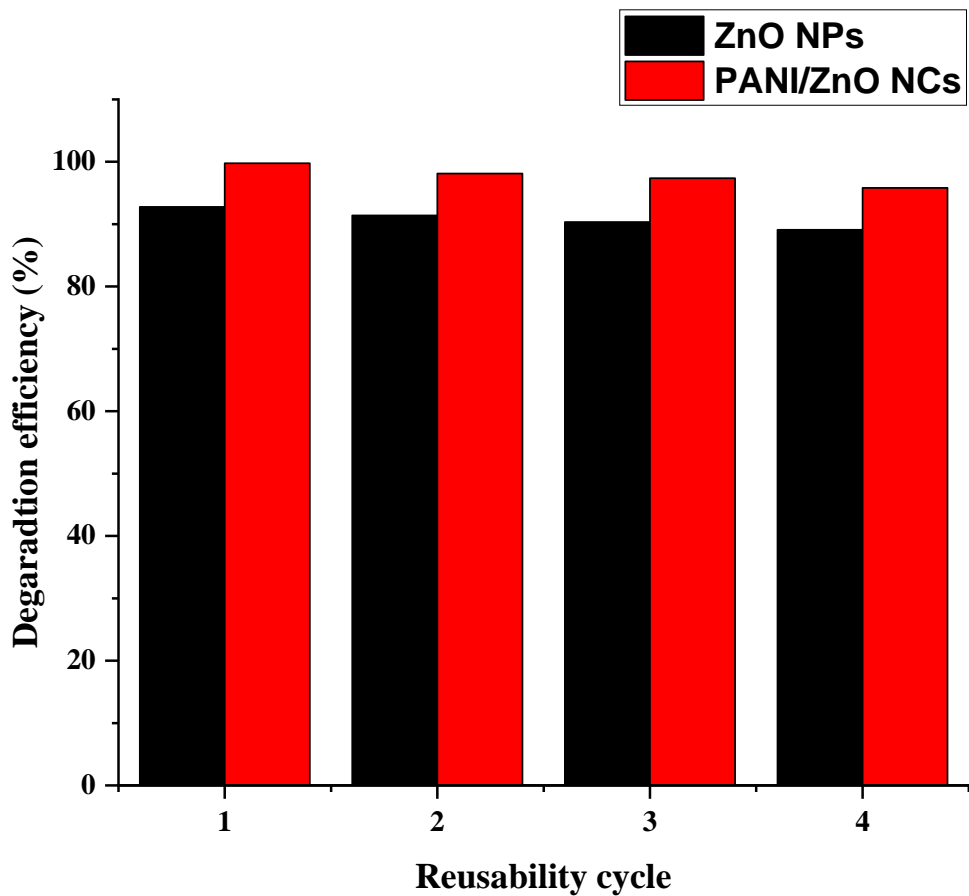


Figure 20: Reusability of ZnO NPs, and PANI/ZnO NCs for the degradation of CV

CHAPTER FIVE

5. CONCLUSION AND RECOMMENDATION

5.1. Conclusion

In conclusion, a PANI/ZnO nanocomposite was successfully synthesized using *Solanecio gigas* leaf extract as a reducing and capping agent for the photocatalytic degradation of Crystal Violet under natural sunlight. Characterization studies using UV-Vis, FT-IR, SEM, and XRD. UV-Vis absorption revealed a type-II heterojunction between PANI and ZnO, with PANI likely reducing the size of ZnO NPs. XRD patterns showed overlapping peaks from the composite with a crystalline size of 5.577 nm, which is smaller than the crystalline size of ZnO NPs (9.455 nm). The effects of experimental conditions such as pH, photocatalyst dosage, and CV concentration were investigated with 91.20% and 99.06% at pH 11, 99.47% and 99.97% at 0.12 g, and 94.93% and 96.20% at 20 ppm for both ZnO NPs and PANI/ZnO NCs. The ZnO/polyaniline nanocomposite exhibited higher photocatalytic activity at 98.25% compared to ZnO nanoparticles at 92.76% under optimal conditions after 60 minutes of sunlight exposure. Kinetics studies indicated that the degradation rate fit well with the pseudo-first-order kinetics model, showing an R^2 value of 0.968 for PANI/ZnO NCs. The PANI/ZnO NCs exhibited good reusability over four cycles, showcasing their potential as sustainable nanocatalysts for environmental remediation.

5.2. Recommendations

Based on the current findings, the following recommendations are forwarded for future research on PANI/ZnO nanocomposites

1. **Explore biological applications:** Investigate the antibacterial, antioxidant, and antimicrobial properties of the nanocomposite.
2. **Evaluate efficacy for industrial wastewater treatment:** Assess the ability of the nanocomposite to degrade a wide range of organic pollutants commonly found in industrial wastewater.

3. **Investigate electrochemical activity:** Study the electrochemical properties of the nanocomposite for potential applications in energy storage and conversion.
4. **Optimize synthesis for scalability:** Determine the feasibility of producing the nanocomposite on a larger scale for practical wastewater treatment applications.

REFERANCE

1. Jara, Y. S., Mekiso, T. T., & Washe, A. P. (2024). Highly efficient catalytic degradation of organic dyes using iron nanoparticles synthesized with Vernonia Amygdalina leafextract. *Scientific Reports*, 14(1), 6997.
2. Eskizeybek, V., Sarı, F., Gülce, H., Gülce, A., & Avcı, A. (2012). Preparation of the new polyaniline/ZnO nanocomposite and its photocatalytic activity for degradation of methylene blue and malachite green dyes under UV and natural sun lights irradiations. *Applied Catalysis B: Environmental*, 119, 197-206.
3. Abomuti, M.A.; Danish, E.Y.; Firoz, A.; Hasan, N.; Malik, M.A. (2021). Green Synthesis of Zinc Oxide Nanoparticles Using Salvia officinalis Leaf Extract and Their Photocatalytic and Antifungal Activities. *Biology*, 10, 1075.
4. Wijesinghe, U.; Thiripuranathar, G.; Mena, F.; Iqbal, H.; Razzaq, A.; Almukhlifi, H. (2021). Green Synthesis, Structural Characterization and Photocatalytic Applications of ZnO Nanoconjugates Using *Heliotropium indicum*. *Catalysts*, 11, 831.
5. Ray, S. S., & Biswas, M. (2000). Water-dispersible conducting nanocomposites of polyaniline and poly (N-vinylcarbazole) with nanodimensional zirconium dioxide. *Synthetic Metals*, 108(3), 231-236.
6. Gemechu, Fikadu Aaga, and Sisay Tadesse Anshebo. (2023)."Green synthesis of highly efficient and stable copper oxide nanoparticles using an aqueous seed extract of Moringa stenopetala for sunlight-assisted catalytic degradation of Congo red and alizarin red s." *Heliyon* 9, 5.
7. Bekru, A.G.; Tufa, L.T.; Zelekew, O.A.; Gwak, J.; Lee, J.; Sabir, F.K. (2023). Microwave-Assisted Synthesis of rGO-ZnO/CuO Nanocomposites for Photocatalytic Degradation of Organic Pollutants. *Crystals*, 13, 133.
8. Sahu, K., Rahamn, K. H., & Kar, A. K. (2019). Synergic effect of polyaniline and ZnO to enhance the photocatalytic activity of their nanocomposite. *Materials Research Express*, 6(9), 095304.
9. Folorunso, O., Olukanmi, P., & Thokozani, S. (2023). Conductive polymers' electronic structure modification for multifunctional applications. *Materials Today Communications*, 106308.
10. Puthukulangara Jaison, J., & Kadanthottu Sebastian, J. (2023). Artemisia stelleriana-

- mediated ZnO nanoparticles for textile dye treatment: a green and sustainable approach. *Water Practice & Technology*, 18(4), 911-921.
11. Sirelkhatim, A., Mahmud, S., Seeni, A., Kaus, N. H. M., Ann, L. C., Bakhori, S. K. M., ... & Mohamad, D. (2015). Review on zinc oxide nanoparticles: antibacterial activity and toxicity mechanism. *Nano-micro letters*, 7, 219-242.
 12. Mohsen, R. M., Morsi, S. M., Selim, M. M., Ghoneim, A. M., & El-Sherif, H. M. (2019). Electrical, thermal, morphological, and antibacterial studies of synthesized polyaniline/zinc oxide nanocomposites. *Polymer Bulletin*, 76, 1-21.
 13. Dessie, Yilkal, Sisay Tadesse, and Rajalakshmanan Eswaramoorthy. (2021) "Surface Roughness and Electrochemical Performance Properties of Biosynthesized α -MnO₂/NiO-Based Polyaniline Ternary Composites as Efficient Catalysts in Microbial Fuel Cells." *Journal of Nanomaterials*: 1-21
 14. Asres, K., Sporer, F. and Wink, M., (2007). Identification and quantification of hepatotoxic pyrrolizidine alkaloids in the Ethiopian medicinal plant *Solanecio gigas* (Asteraceae). *Die Pharmazie-An International Journal of Pharmaceutical Sciences*, 62(9), 709-713.
 15. A. ur Rehman et al., (2021). Fabrication of binary metal doped CuO nanocatalyst and their application for the industrial effluents treatment, *Ceramics International*, . 47, 5. Elsevier Ltd, . 5929–5937
 16. Roberson, M.; Rangari, V.; Jeelani, S.; Samuel, T.; Yates, C. (2014). Synthesis and Characterization Silver, Zinc Oxide and Hybrid Silver/Zinc Oxide Nanoparticles for Antimicrobial Applications. *Nano Life.*, 4, 1440003.
 17. Ahmad, K. S.; Jaffri, S. B. (2018) Phytosynthetic Ag Doped ZnO Nanoparticles: Semiconducting Green Remediators. *Open Chemistry.*, 16, 556–570.
 18. Khaldakar, M.; Butala, D. (2017) The Synthesis and Characterization of Metal Oxide Nanoparticles and its Application for Photocatalysis. *International Journal of Scientific and Research Publications.*, 7, 499-504.
 19. Saeed, M.; Muneer, M.; Khosa, M. K. K.; Akram, N.; Khalid, S.; Adeel, M.; Nisa, A.; Sherazi, S. (2019) Azadirachta Indica Leaves Extract Assisted Green Synthesis of Ag-TiO₂ for Degradation of Methylene Blue and Rhodamine B Dyes in Aqueous Medium. *Green Processing and Synthesis.*, 8, 659-666.
 20. Abrahart, E. N. (1977). *Dyes and their intermediates.*

21. Bafana, A., Devi, S.S. and Chakrabarti, T. (2011) Azo dyes: past, present and the future. *Environmental Reviews*,. 19(NA): 350
22. Taqui, S. N., Cs, M., Goodarzi, M. S., Elkotb, M. A., Khatoon, B. A., Soudagar, M. E. M., ... & Saleel, C. A. (2021). Sustainable adsorption method for the remediation of crystal violet dye using nutraceutical industrial fenugreek seed spent. *Applied Sciences*, 11(16), 7635.
23. Loulidi, I., Jabri, M., Amar, A., Kali, A., A. Alrashdi, A., Hadey, C., ... & Boukhelifi, F. (2023). Comparative study on adsorption of crystal violet and Chromium (VI) by activated carbon derived from spent coffee grounds. *Applied Sciences*, 13(2), 985.
24. Prathna, T., Mathew, L., Chandrasekaran, N. and Raichur, A. M. (2010) Biomimetic synthesis of nanoparticles: science, technology & applicability, in *Biomimetics learning from nature*., InTech.
25. Niemann, B., Rauscher, F., Adityawarman, D., Voigt, A. and Sundmacher, K . (2006.) Microemulsion-assisted precipitation of particles: Experimental and model-based process analysis. *Chemical Engineering and Processing: Process Intensification*, 45(10): 917.
26. Sharma, D., Rajput, J., Kaith, B. S., Kaur, M. and Sharma, S. (2010) Synthesis of ZnO nanoparticles and study of their antibacterial and antifungal properties. *Thin solid films*. 519(3): 1224.
27. Auffan, M., Rose, J., Bottero, J.Y., Lowry, G.V., Jolivet, J.P., Wiesner, M.R. (2009) Towards a definition of inorganic nanoparticles from an environmental, health and safety perspective. *Nature nanotechnology*,. 4(10): 634
28. Tiwari, D.K., Behari, J. and Prasenjit Sen, P.S., (2008). Application of nanoparticles in waste water treatment.
29. Mansha, M., Khan, I., Ullah, N. and Qurashi, A., (2017). Synthesis, characterization and visible-light-driven photoelectrochemical hydrogen evolution reaction of carbazole-containing conjugated polymers. *International Journal of Hydrogen Energy*, 42(16), .10952-10961.
30. Dreaden, E.C., Alkilany, A.M., Huang, X., Murphy, C.J. and El-Sayed, M.A., (2012). The golden age: gold nanoparticles for biomedicine. *Chemical Society Reviews*, 41(7), 2740-2779
31. Salavati-Niasari, M., Davar, F. and Mir, N., (2008). Synthesis and characterization of

- metallic copper nanoparticles via thermal decomposition. *Polyhedron*, 27(17), .3514-3518.
32. Tai, C.Y., Tai, C.T., Chang, M.H. and Liu, H.S., (2007). Synthesis of magnesium hydroxide and oxide nanoparticles using a spinning disk reactor. *Industrial & engineering chemistry research*, 46(17), .5536-5541.
 33. Thomas, S. C, Kumar Mishra, P. and Talegaonkar, S., (2015). Ceramic nanoparticles: fabrication methods and applications in drug delivery. *Current pharmaceutical design*, 21(42), .6165-6188.
 34. Sabir, S., Arshad, M. and Chaudhari, S.K. (2014). Zinc oxide nanoparticles for revolutionizing agriculture: synthesis and applications. *The Scientific World Journal*,.
 35. Behera, O. (2008.) Synthesis and Characterization of ZnO nanoparticles of various sizes and Applications in Biological systems (Doctoral dissertation, National Institute of Technology Rourkela).
 36. Singh, A., Singh, N. Á., Afzal, S., Singh, T., & Hussain, I. (2018). Zinc oxide nanoparticles: a review of their biological synthesis, antimicrobial activity, uptake, translocation and biotransformation in plants. *Journal of materials science*, 53(1), 185-201.
 37. Lee, G., Lee, B., & Kim, K. T. (2021). Mechanisms and effects of zinc oxide nanoparticle transformations on toxicity to zebrafish embryos. *Environmental Science: Nano*, 8(6), 1690-1700.
 38. Al Jabri, H., Saleem, M. H., Rizwan, M., Hussain, I., Usman, K., & Alsafran, M. (2022). Zinc oxide nanoparticles and their biosynthesis: overview. *Life*, 12(4), 594.
 39. Bedre, Mahesh D., et al. (2012). "Preparation and characterization of polyaniline-Co₃O₄ nanocomposites via interfacial polymerization." *Am. J. Mater. Sci* 2.3 3943.
 40. Ryu, S.K., Kim, M.K., Park, G.N., Park, J.Y. and Chang, H.S. (2002). Hydrophilic polyaniline nanofibrous architecture using electrosynthesis method for supercapacitor application. *Journal of Power Source*, 103: 305-309.
 41. Ruecha, N., Rodthongkum, N., Cate, D.M., Volckens, J., Chailapakul, O. and Henry, C.H.(2015). Sensitive electrochemical sensor using a graphene–polyaniline nanocomposite for simultaneous detection of Zn(II), Cd(II), and Pb(II). *Journal of Chemical Engineering*, 874: 40–48
 42. Alamgeer; Tahir, M.; Sarker, M.R.; Ali, S.; Ibraheem; Hussian, S.; Ali, S.; Imran Khan, M.; Khan, D.N.; Ali, R.; et al. (2023) Polyaniline/ZnO Hybrid Nanocomposite: Morphology,

- Spectroscopy and Optimization of ZnO Concentration for Photovoltaic Applications. *Polymers*, 15, 363.
43. Turkten, N.; Karatas, Y.; Bekbolet, M. (2021,) Preparation of PANI Modified ZnO Composites via Different Methods: Structural, Morphological and Photocatalytic Properties. *Water* 13, 1025
 44. S. Kandasamy and R. Sorna Prema. (2015) Methods of synthesis of nano particles and its applications. *Journal of Chemical and Pharmaceutical Research*, , 7(3):278-285
 45. Singh, J.et al. (2018), Green synthesis of metals and their oxide nanoparticles: Applications for environmental remediation. *Journal of Nanosbiotechnology*, 16(1), 1–24.
 46. Shafey, A. (2020) Green synthesis of metal and metal oxide nanoparticles from plant leaf extracts and their applications: A review. *Green Processing and Synthesis*, , 9(1), 304–339
 47. Molla Yitayeh, M., & Monie Wassihun, A. (2022). Chemical composition and antibacterial and antioxidant activities of stem bark essential oil and extracts of *Solanecio gigas*. *Biochemistry Research International*, 2022.
 48. Tahoun, B. A., Farag, E. M., Tony, M. A., & Mansour, S. A. (2023). Feasibility analysis of synthesized polyaniline nanocomposites loaded by Co-doped ZnO nanorods for aqueous pollutants oxidation. *Applied Water Science*, 13(12), 225.
 49. Asres, K., Sporer, F. and Wink, M., (2008). Occurrence of pyrrolizidine alkaloids in three Ethiopian *Solanecio* species. *Biochemical Systematics and Ecology*, 36(5-6), 399-407M.T.
 50. Asres, K., Sporer, F. and Wink, M., (2007). Identification and quantification of hepatotoxic pyrrolizidine alkaloids in the Ethiopian medicinal plant *Solanecio gigas* (Asteraceae). *Die Pharmazie-An International Journal of Pharmaceutical Sciences*, 62(9), 709-713.
 51. Noori, B.R. Tiwari, M.M. Ghangrekar, B. (2019) Min, *Azadirachta indica* leaf extract-assisted synthesis of Co-NiO mixed metal oxide for application in a microbial fuel cell as a cathode catalyst, *Sustain. Energy Fuels* 3 3430–3440.
 52. U.G.Akpan,B.H. (2009) Hameed.Parametrs affecting photocatalytic degradation of dyes using TiO₂ – basedphotocatalysts: A review. *journal of hazardous material.*,170,520-529
 53. Gowland, D.C.A.; Robertson, N.; Chatzisyneon, E. (2021) Photocatalytic Oxidation of Natural Organic Matter in Water. *Water*, 13, 288.
 54. Kumar A, Pandey G. (2017) Photodegradation of Methyl Orange in Aqueous Solution by the Visible Light Active Co: La: TiO₂ Nanocomposite. *Chem Sci J.*, 8,164.V

55. Cavigli L, et al. (2009) Volume versus surface-mediated recombination in anatase TiO₂ nanoparticles. *Journal of Applied Physics*. 106(5), 053516.
56. Coleman HM, et al. (2007) Degradation of 1,4-dioxane in water using TiO₂ based photocatalytic and H₂ O₂ / UV processes. *J Hazard Mater.*; 146(3):496–501.
57. S. Ahmed, et al. (2011) Influence of parameters on the heterogeneous photocatalytic degradation of pesticides and phenolic contaminants in waste water: A short review, *J. Environ. Manage.* 92, 311-330.
58. Naiel, B., Fawzy, M., Halmy., M.W.A. and Mahmoud, A.E.D. (2022). Green synthesis of zinc oxide nanoparticles using Sea Lavender (*Limonium pruinosum* L. Chaz.) extract: characterization, evaluation of anti-skin cancer, antimicrobial and antioxidant potentials. *Scientific Reports*, 12(1), 20370.
59. Meena, P.L. and Saini, J.K., (2023). Synthesis of polymer-metal oxide (PANI/ZnO/MnO₂) ternary nanocomposite for effective removal of water pollutants. *Results in Chemistry*, 5, p.100764.
60. Firisa, S.G., Muleta, G.G. and Yimer, A.A., (2022). Synthesis of nickel oxide nanoparticles and copper-doped nickel oxide nanocomposites using *Phytolacca dodecandra* l'herit leaf extract and evaluation of its antioxidant and photocatalytic activities. *ACS omega*, 7(49), pp.44720-44732.
61. Yadeta Gemachu, L., & Lealem Birhanu, A. (2024). Green synthesis of ZnO, CuO and NiO nanoparticles using Neem leaf extract and comparing their photocatalytic activity under solar irradiation. *Green Chemistry Letters and Reviews*, 17(1), 2293841.
62. Panchal, P., Paul, D. R., Sharma, A., Hooda, D., Yadav, R., Meena, P., & Nehra, S. P. (2019). Phytoextract mediated ZnO/MgO nanocomposites for photocatalytic and antibacterial activities. *Journal of Photochemistry and Photobiology A: Chemistry*, 385, 112049.
63. Karam, S. T., & Abdulrahman, A. F. (2022, August). Green synthesis and characterization of ZnO nanoparticles by using thyme plant leaf extract. In *Photonics* (. 9, 8, 594). MDPI.
64. Muhammad, W., Ullah, N., Haroon, M., & Abbasi, B. H. (2019). Optical, morphological and biological analysis of zinc oxide nanoparticles (ZnO NPs) using *Papaver somniferum* L. *RSC advances*, 9(51), 29541-29548.

65. Y. Dessie, S. Tadesse, and Y. Adimasu, (2022) “Improving the performance of graphite anode in a Microbial Fuel Cell via PANI encapsulated α -MnO₂ composite modification for efficient power generation and methyl red removal,” *Chem. Eng. J. Adv.*, 10, 2022,
66. Hassan, S. S., El Azab, W. I., Ali, H. R., & Mansour, M. S. (2015). Green synthesis and characterization of ZnO nanoparticles for photocatalytic degradation of anthracene. *Advances in Natural Sciences: Nanoscience and Nanotechnology*, 6(4), 045012.
67. K. I. Ajeel, and Q. S. Kareem, (2019) “synthesis and characteristics of polyaniline (PANI) filled by graphene (PANI/GR) nano-films,” *J. Phys. Conf. Ser.*, 1088/1742-6596/1234/1/012020
68. Ge, B., Xu, Y., Zhao, H., Sun, H., Guo, Y., & Wang, W. (2018). High performance gas separation mixed matrix membrane fabricated by incorporation of functionalized submicrometer-sized metal-organic framework. *Materials*, 11(8), 1421.
69. Hassan, S. A., Hamzah, M. Q., & Agam, M. A. (2022, June). Conductivity of PANI/ZnO Nanocomposites. In *Proceedings of the 7th International Conference on the Applications of Science and Mathematics: Sciematic* (. 107-113). Singapore: Springer Nature Singapore. Optical and Structural Properties of Zinc Oxide Nanoparticles..
70. Meruvu, H., Vangalapati, M., Chippada, S. C., & Bammidi, S. R. (2011). Synthesis and characterization of zinc oxide nanoparticles and its antimicrobial activity against *Bacillus subtilis* and *Escherichia coli*. *J. Rasayan Chem*, 4(1), 217-222.
71. M. Usman et al., (2021) “In Situ Synthesis of a Polyaniline/ Fe–Ni Co doped Co₃O₄ Composite for the Electrode Material of Super capacitors with Improved Cyclic Stability,” *ACS omega*, 6, .1190–1196, ,
72. X. Zhu et al., (2019) “In-situ modulation of interactions between polyaniline and graphene oxide films to develop waterborne epoxy anticorrosion coatings,” *Prog. Org. Coatings* vol.133, 5, 106–116, j.progcoat.2019.04.016
73. Charpe, SD, F.C. Raghuwanshi (2016). “Synthesis and Structural Properties of Nanocomposite of pani/zno by in situ polymerization” *Research journal of Chemical science*.. 6(5), 1-11
74. Alamgeer, Tahir, M., Sarker, M. R., Ali, S., Ibraheem, Hussian, S., ... & Mohd Said, S. (2023). Polyaniline/ZnO Hybrid Nanocomposite: Morphology, Spectroscopy and Optimization of ZnO Concentration for Photovoltaic Applications. *Polymers*, 15(2), 363.

75. Nosrati, R., Olad, A., & Maramifar, R. (2012). Degradation of ampicillin antibiotic in aqueous solution by ZnO/polyaniline nanocomposite as photocatalyst under sunlight irradiation. *Environmental Science and Pollution Research*, *19*, 2291-2299.
76. Özbay, B., Genç, N., Özbay, İ., Bağhaki, B., & Zor, S. (2016). Photocatalytic activities of polyaniline-modified TiO₂ and ZnO under visible light: an experimental and modeling study. *Clean Technologies and Environmental Policy*, *18*, 2591-2601.
77. Olad, A., & Nosrati, R. (2012). Preparation, characterization, and photocatalytic activity of polyaniline/ZnO nanocomposite. *Research on Chemical Intermediates*, *38*, 323-336.
78. Vijayalakshmi, S., Kumar, E., Ganeshbabu, M., Venkatesh, P. S., & Rathnakumar, K. (2021). Structural, electrical, and photocatalytic investigations of PANI/ZnO nanocomposites. *Ionics*, *27*, 2967-2977.
79. Rani, M., Yadav, J., Shanker, U., & Sillanpää, M. (2023). Green synthesized zinc derived nanocomposites with enhanced photocatalytic activity: An updated review on structural modification, scientific assessment and environmental applications. *Inorganic Chemistry Communications*, *147*, 110246.
80. Supin, K. K., PM, P. N., & Vasundhara, M. (2023). Enhanced photocatalytic activity in ZnO nanoparticles developed using novel *Lepidagathis ananthapuramensis* leaf extract. *RSC advances*, *13*(3), 1497-1515.
81. Tababouchet, M. Y., Sakri, A., Bouremel, C., & Boutarfaia, A. (2023, December). Synthesis of Polyaniline-Zinc Oxide Composites: Assessment of Structural, Morphological, and Electrical Properties. In *Annales de Chimie Science des Matériaux* (. 47, 6).

APPENDICES

Appendix 1: Effect of pH

Photocatalytic degradation condition of CV with 5 ppm of initial conc. CV, 0.02 g of nano-photocatalyst dosage, $A_0 = 0.636$ and Exposure time = 60 min

pH	Trials	Pure ZnO NPs		PANI/ZnO NCs	
		Abs	Degradation efficiency (%)	Abs	Degradation efficiency (%)
2	1	0.570		0.478	
	2	0.567		0.478	
	3	0.576		0.480	
	A _{av}	0.571	10.36% ± 0.00458	0.477	25.1% ± 0.00115
3	1	0.530		0.426	
	2	0.531		0.424	
	3	0.531		0.4245	
	A _{av}	0.531	16.55% ± 0.00057	0.4245	33.35% ± 0.0011
4	1	0.489		0.372	
	2	0.489		0.372	
	3	0.488		0.371	
	A _{av}	0.489	23.24% ± 0.00057	0.372	41.56% ± 0.0057
5	1	0.445		0.326	
	2	0.446		0.326	
	3	0.446		0.327	
	A _{av}	0.445	30.01% ± 0.00057	0.326	48.74% ± 0.0057
6	1	0.397		0.269	
	2	0.399		0.271	
	3	0.398		0.267	
	A _{av}	0.399	37.29% ± 0.001	0.269	57.63% ± 0.002
	1	0.345		0.220	

7	2	0.343		0.218	
	3	0.345		0.218	
	A _{av}	0.344	45.92%±0.00115	0.219	65.51%±0.0011
8	1	0.288		0.161	
	2	0.289		0.162	
	3	0.288		0.160	
	A _{av}	0.288	54.75%±0.00057	0.161	74.64%±0.001
9	1	0.221		0.108	
	2	0.220		0.107	
	3	0.222		0.105	
	A _{av}	0.221	65.18%±0.001	0.107	83.05%±0.0015
10	1	0.153		0.049	
	2	0.153		0.047	
	3	0.155		0.048	
	A _{av}	0.153	75.84%±0.00115	0.048	92.56%±0.001
11	1	0.055		0.019	
	2	0.055		0.016	
	3	0.058		0.019	
	A _{av}	0.056	91.19%±0.00173	0.018	99.06%±0.0017
12	1	0.093		0.025	
	2	0.092		0.026	
	3	0.092		0.026	95.81%±0.0005
	A _{av}	0.092	88.43%±0.00057	0.065	
13	1	0.097		0.065	
	2	0.098		0.069	
	3	0.096		0.066	89.57%±0.0023
	A _{av}	0.097	82.64%±0.001	0.113	
	1	0.138		0.113	
	2	0.137		0.114	
	3	0.135		0.113	82.22%±0.0005

14	A_{av}	0.137	$78.39\% \pm 0.00152$	0.026	
-----------	----------	-------	-----------------------	-------	--

Values are triplicate mean of degradation efficiency \pm standard deviation

Appendix 2: Effect of Photocatalytic Dosage

Photocatalytic degradation condition of CV with 5 ppm of initial conc. CV, with optimized pH at 11 for ZnO NPs and 11 for PANI/ZnO NCs, respectively, $A_0 = 0.636$, and Exposure time = 1 hr

Photo-catalyst dosage (g)	Trials	Pure ZnO NPs		PANI/ZnO NCs	
		Absorbance ($A_{t=1hr}$)	Degradation efficiency (%)	Absorbance ($A_{t=1hr}$)	Degradation efficiency (%)
0.04	1	0.038		0.011	
	2	0.039		0.013	
	3	0.040		0.009	
	A_{av}	0.039	93.88%±0.0005	0.011	98.21%±0.002
0.08	1	0.034		0.004	
	2	0.034		0.004	
	3	0.030		0.003	
	A_{av}	0.033	94.72%±0.002	0.004	99.36%±0.0005
0.12	1	0.003		0.0001	
	2	0.003		0.0001	
	3	0.004		0.0001	
	A_{av}	0.003	99.47%±0.0005	0.0001	99.97%±0.0001
0.16	1	0.007		0.004	
	2	0.010		0.005	
	3	0.009		0.004	
	A_{av}	0.009	98.55%±0.0015	0.004	99.29%±0.0005
0.2	1	0.014		0.01	
	2	0.013		0.02	
	3	0.012		0.01	
	A_{av}	0.013	97.83%±0.001	0.01	98.68%±0.0005

Values are triplicate mean of degradation efficiency ± standard deviation

Appendix 3: Effect of Initial Concentration of CV

Photocatalytic degradation condition of CV at optimal photocatalyst dosage 0.12 g for both ZnO NPs PANI/ZnO NCs and at with optimized pH at 11 for pure ZnO NPs and 11 for PANI/ZnO NCs, respectively and Exposure time = 1 hr.

Initial conc. of CV (ppm)	A ₀	Trials	Pure ZnO NPs		PANI/ZnO NCs	
			Absorbance (A _{t=1hr})	Degradation efficiency (%)	Absorbance (A _{t=1hr})	Degradation efficiency (%)
5	2.231	1	0.023		0.016	
		2	0.018		0.016	
		3	0.024		0.017	
		A _{av}	0.022	99.01% ± 0.00321	0.016	99.28% ± 0.0058
10	1.760	1	0.040		0.046	
		2	0.041		0.047	
		3	0.041		0.045	
		A _{av}	0.041	97.67 ± 0.0058	0.046	98.38% ± 0.001
15	2.693	1	0.073		0.106	
		2	0.073		0.105	
		3	0.070		0.107	
		A _{av}	0.072	97.29% ± 0.00458	0.106	96.06% ± 0.00436
20	1.107	1	0.041		0.046	
		2	0.042		0.039	
		3	0.049		0.040	
		A _{av}	0.045	94.93% ± 0.00436	0.042	96.20% ± 0.00379
25	0.636	1	0.106		0.038	
		2	0.107		0.039	
		3	0.106		0.037	
		A _{av}	0.106	83.29% ± 0.00208	0.038	87.03% ± 0.0058

Values are triplicate mean of degradation efficiency ± standard deviation

Appendix 4: Effect of Reaction Time

Photocatalytic degradation of crystal violet by ZnO NPs and PANI/ZnO NCs, degradation condition of crystal violet kept at optimal point for others parameters with different reaction time.

Nano-catalyst		Pure ZnO NPs		PANI/ZnO NCs	
Exposure time (min)	Absorbance ($A_{t=1hr}$)	Absorbance at time t. (A_t)	Degradation efficiency (%)	Absorbance at time t. (A_t)	Degradation efficiency (%)
10	1	1.999		1.824	
	2	1.997		1.823	
	3	1.999		1.820	
	A_{av}	1.999	10.35±0.00115	1.822	18.30±0.002081
20	1	1.741		1.485	
	2	1.741		1.486	
	3	1.743		1.487	
	A_{av}	1.742	21.89±0.00115	1.486	33.31±0.001
30	1	1.473		1.205	
	2	1.475		1.204	
	3	1.471		1.205	
	A_{av}	1.473	51.94±0.002	1.205	45.94±0.000577
40	1	0.816		0.529	
	2	0.818		0.528	
	3	0.819		0.526	
	A_{av}	0.817	63.35%±0.00152	0.528	70.37%±0.00057
50	1	0.424		0.019	
	2	0.426		0.017	
	3	0.426		0.019	
	A_{av}	0.426	78.89%±0.00115	0.019	84.33%±0.00057
	1	0.094		0.004	

60	2	0.093		0.005	
	3	0.095		0.005	
	A_{av}	0.094	92.76%±0.001	0.005	98.25%±0.00577
70	1	0.08		0.0053	
	2	0.081		0.0052	
	3	0.081		0.0053	
	A_{av}	0.080	93.38%±0.00577	0.0053	99.74%±0.00005
80	1	0.055		0.0051	
	2	0.058		0.0051	
	3	0.058		0.0052	
	A_{av}	0.057	93.41%±0.00173	0.0051	99.78%±0.00005

Values are triplicate mean of degradation efficiency ± standard deviation

Appendix 5: Calibration Curve Data

Initial conc. of CV (ppm)	Triplicate	Abs (A₀)	Average Absorbance (A_v A₀)	Standard deviation (SD)
5	1	0.638	0.636	±0.00208
	2	0.635		
	3	0.639		
10	1	1.107	1.107	±0.0058
	2	1.106		
	3	1.106		
15	1	1.762	1.761	±0.00173
	2	1.762		
	3	1.759		
20	1	2.231	2.232	±0.00153
	2	2.229		
	3	2.232		
25	1	2.695	2.693	±0.00306
	2	2.691		
	3	2.689		

Values are triplicate mean of absorbance for initial concentration ± standard deviation

Appendix 6: Kinetic Data

Data for calculation of the dyes at different reaction time A_0 2.231 for both ZnO NPs and PANI/ZnO NCs for CV photocatalytic degradation

Kinetics study Models					Zero-Order		First-Order	Second-Order
Nano catalyst	Time (t) (min)	Abs at time t. (A_t)	C_0 (ppm)	C_t (ppm)	$C_0 - C_t$	$\frac{C_0}{C_t}$	$\ln \frac{C_0}{C_t}$	$\frac{1}{C_t} - \frac{1}{C_0}$
Pure ZnO NPs	10	0.059	20	0.570	19.430	35.085	3.558	1.704
	20	0.047	20	0.454	19.546	44.042	3.785	2.152
	30	0.041	20	0.396	19.604	50.488	3.922	2.474
	40	0.036	20	0.348	19.652	57.500	4.052	2.825
	50	0.022	20	0.212	19.787	94.091	4.544	4.654
	60	0.005	20	0.048	19.952	414	6.0258	20.65
PANI/ZnO NCs	10	0.027	20	0.261	19.739	76.666	4.3395	3.7833
	20	0.015	20	0.145	19.855	138	4.9272	6.85
	30	0.012	20	0.116	19.884	172.5	5.1504	8.575
	40	0.01	20	0.097	19.903	207	5.3327	10.3
	50	0.005	20	0.048	19.952	414	6.0258	20.65
	60	0.004	20	0.039	19.961	517.5	6.2490	25.825

Appendix 7: Catalyst Reusability

Reusability and stability test of ZnO NPs and PANI/ZnO NCs for the photocatalytic degradation of CV at optimum condition

Nano-catalyst		ZnO NPs		PANI/ZnO NCs	
Number of cycles	Trial	Abs ($A_{t=60 \text{ min}}$)	Degradation efficiency (%)	Abs ($A_{t=60 \text{ min}}$)	Degradation efficiency (%)
First	1	0.094		0.005	
	2	0.094		0.005	
	3	0.095		0.004	
	A_{av}	0.094	92.76±0.000577	0.005	99.75±0.000577
Second	1	0.123		0.031	
	2	0.122		0.030	
	3	0.124		0.028	
	A_{av}	0.124	91.41±0.0001	0.030	98.11±0.001528
Third	1	0.172		0.058	
	2	0.170		0.059	
	3	0.169		0.057	
	A_{av}	0.170	90.35±0.001527	0.058	97.36±0.0001
Fourth	1	0.223		0.093	
	2	0.220		0.093	
	3	0.220		0.093	
	A_{av}	0.221	89.09±0.001732	0.092	95.82±0.000577

Values are triplicate mean of degradation efficiency ± standard deviation

